

Citation for published version:
Karmakar, S, Kiran, R, Ansari, MNM, Yakout, SM, Thomas, P, Vaish, R, Singh Chauhan, V & Bowen, C 2022, 'Negative Poisson's ratio polyethylene matrix and 0.5BaCa0.8Zr0.2O3-0.5Ba0.7Ca0.3TiO3 based piezocomposite for sensing and energy harvesting applications', Polymers.

Publication date: 2022

Document Version Peer reviewed version

Link to publication

Publisher Rights CC BY

University of Bath

Alternative formats

If you require this document in an alternative format, please contact: openaccess@bath.ac.uk

General rights

Copyright and moral rights for the publications made accessible in the public portal are retained by the authors and/or other copyright owners and it is a condition of accessing publications that users recognise and abide by the legal requirements associated with these rights.

If you believe that this document breaches copyright please contact us providing details, and we will remove access to the work immediately and investigate your claim.

Download date: 08. Mar. 2023





Article

Negative Poisson's ratio polyethylene matrix and $0.5Ba(Ca_{0.8}Zr_{0.2})O_3 - 0.5(Ba_{0.7}Ca_{0.3})TiO_3$ based piezocomposite for sensing and energy harvesting applications

Saptarshi Karmakar¹, Raj Kiran², M.N.M.Ansari^{3*}, Sobhy M. Ibrahim⁴, P.Thomas⁵, Rahul Vaish^{1*}, Vishal Singh Chauhan¹ and Chris Bowen⁶

¹School of Engineering, Indian Institute of Technology Mandi, Himachal Pradesh, 175075, India

Abstract: Finite element studies were conducted on $0.5Ba(Ca_{0.8}Zr_{0.2})0_3 - 0.5(Ba_{0.7}Ca_{0.3})TiO_3$ (BCZ-BCT) piezoelectric particles embedded in polyethylene matrix to create a piezocomposite having a positive and negative Poisson's ratio of -0.32 and 0.2. Polyethylene with a positive Poisson's ratio is referred to as non-auxetic while those with negative Poisson's ratio are referred to as auxetic or inherently auxetic. The effective elastic and piezoelectric properties were calculated at volume fractions of (4%, 8% to 24%) to study their sensing and harvesting performance. Auxetic piezocomposite demonstrated an overall improvement in performance in terms of higher sensing voltage and harvested power. The study was repeated at a constant volume fraction of 24% for a range of Poisson's ratio varied between -0.9 to 0.4. Enhanced performance was observed at the extreme negative end of the Poisson's ratio spectrum. This paper demonstrates the potential improvements by exploiting auxetic matrices in future piezocomposite sensors and energy harvesters.

Keywords: Piezocomposites; Auxetic; Non-auxetic; Sensing; Energy Harvesting; Finite Element Modeling

M.N.M.Ansari3*; Ibrahim, S.M.; P.Thomas5; Vaish, R.; Chauhan, V.S.; Bowen, C. Improved sensing and energy harvesting performance of $0.5Ba(Ca_{0.8}Zr_{0.2})O_3 - 0.5(Ba_{0.7}Ca_{0.3})TiO_3$ piezoceramics using inherently auxetic polyeth-

Citation: Karmakar, S.; Kiran, R.;

Academic Editor(s):

vlene matrix.

Received: date Accepted: date Published: date

Publisher's Note: MDPI stays neutral with regard to jurisdictional claims in published maps and institutional affiliations.



Copyright: © 2021 by the authors. Submitted for possible open access publication under the terms and conditions of the Creative Commons Attribution (CC BY) license (http://creativecommons.org/licenses/by/4.0/).

1. Introduction

The trends in the electronic industries have always been to reduce their size and power requirements while increasing their functionality. Such endeavors have resulted in low-power microelectronic devices, which are gaining widespread applications in electronic industries[1]. Such devices can be powered by a variety of electrical energy storage(EES) devices like batteries, supercapacitors, chemical storage devices, fuel cells etc [2]. Recent developments like porous natural wood and Li-Na based supercapacitors with high energy density (31.88 $Whkg^{-1}$) can led to prolonged use of this microelectronic devices[3]. Several other recent developments in the field of energy storage has also increased the use of these microelectronic devices [4-8]. In addition to the energy storage devices, however, due to their low power requirements, energy harvesting devices, energy harvested from ambient sources can also be used as an auxiliary power source. A range of energy harvesting techniques such as photovoltaic, piezoelectric, pyroelectric, thermoelectric, and electromagnetic have been explored and reported in the

²School of Mechanical and Aerospace Engineering, Nanyang Technological University, 50 Nanyang Avenue, Singapore 639798, Singapore

³Institute of Power Engineering, Universiti Tenaga Nasional, Kajang 43000, Selangor, Malaysia.

⁴Department of Biochemistry, College of Science, King Saud University, P.O. Box: 2455, Riyadh 11451, Saudi Arabia

⁵Central Power Research Institute, Dielectric Materials Division Bengaluru, Karnataka, India, 560080

⁶Department of Mechanical Engineering, University of Bath, Bath, BA2 7AY, UK

^{*} Correspondence: ansari@uniten.edu.my, rahul@iitmandi.ac.in; Phone: +91-1905-267139

46

47

48

49

50

51

52

53

54

55

56

57

59

60

61

62

63

64

65

66

68

69

70

71

72

73

74

75

76

77

78

79

80

81

82

83

84

85

86

87

88

89

90

91

92

93

94

95

96

97

98

literature[1, 9]. Piezoelectric energy harvesters are devices that convert ambient vibrational energy into electrical energy, and vice-versa, and usually operate in a low vibrational frequency range of ~ 1 - 100 Hz [10-13]. A piezoelectric material, which can convert mechanical energy into electrical energy and vice-versa, is specifically used for this purpose[14]. Piezoelectric materials generally have a remnant polarization due to charge separation in the crystal structure. Under the influence of an externally applied load, a potential difference is produced by the direct piezoelectric effect due to a change in polarization of the material. The opposite phenomenon is often referred to as the converse piezoelectric effect, where a strain is developed due to an applied electric field. A range of piezoelectric materials demonstrates this phenomenon in which piezoelectric materials can be used in bulk material form, as piezoelectric ceramics, or in composite form as piezocomposites. Piezoceramics can exhibit superior properties in terms of high piezoelectric coefficients but are high density, rigid, brittle, and generally have high acoustic impedance. Piezocomposites, therefore, are generally preferred for sensing and energy harvesting applications for their flexibility, toughness, and ease of manufacturing [15-17], where several such piezocomposites have already been reported in the literature [18, 19]. Since piezoelectric energy harvester harvests vibrational energy, a host vibrational device is required to which the piezocomposite can be attached. Kim et al. [20] reported on the different types of vibrating devices such as stacks, shells, cymbals, and cantilevers. In the present study, a cantilever beam-type energy harvester is considered and the piezocomposite material is attached to the cantilever beam energy harvester either in a unimorph or bimorph configuration [15, 16, 21, 22].

A range of piezoelectric materials has been reported in the literature such as polycrystalline ceramics, single-crystal materials, etc. Priya et al.[13] investigated different lead-based and lead-free piezoelectric materials. Lead-based piezoelectric materials such $Pb(Mg_{1/3}Nb_{2/3})O_3 - PbTiO_3$ (PMN-PT), $Pb[Zr_xTi_{1-x}]O_3$ (PZT-5A), $Pb(Zn_{1/3}Nb_{2/3})O_3 - (6 - 7\%)PbTiO_3$ (PZN-PT) are more popular due to their high piezoelectric coefficient. However, lead is toxic both to humans and to the environment. This has led to an interest in the development of non-toxic lead-free piezoelectric materials [23-25] and lead-free piezoelectric materials such as $(Bi_{0.5}Na_{0.5})TiO_3$ [BNT], sodium potassium niobate $(K_{0.5}Na_{0.5})NbO_3$ [KNN], bismuth potassium titanate (Bi_{0.5}K_{0.5})TiO₃ [BKT], and barium zirconate titanate-barium calcium titanate $0.5Ba(Ca_{0.8}Zr_{0.2})O_3 - 0.5(Ba_{0.7}Ca_{0.3})TiO_3$ [BCZ-BCT][26] have been reported in the literature. The large piezoelectric coefficient of BCZ-BCT makes it a promising piezoelectric material for sensing and energy harvesting applications[27].

Various means have been devised to improve the piezoelectric performance and sensing and energy harvesting capabilities of piezoceramics and piezocomposites. For example, Zhang et al. [28] reduced the dielectric loss and enhanced the performance of the BCZ-BCT material by inducing porosity in the BCZ-BCT material. Kiran et al.[29] improved sensing and energy harvesting performance of a KNLNTS and PVDF-based piezocomposite by imparting porosity into it and Karmakar et al. [30] also improved the sensing and energy harvesting capabilities of a BCZ-BCT piezoceramic using porosity. Wang et al.[31] enhanced the piezoelectric properties of BCZ-BCT ceramics by optimizing the calcination and sintering temperature of the manufacturing process and Karmakar et al.[32] studied the effect of sintering temperature on sensing and energy harvesting performance of BCZ-BZT piezoceramic sintered at different temperatures. For the past three decades, metamaterials have received significant attention from the research community. Metamaterials are superior materials that possess counterintuitive and unusual properties in various aspects such as density[33], heat transport [34, 35], and negative Poisson's ratio (NPR) material [36, 37]. Lakes [38] was the first to report the existence of a negative Poisson's ratio (NPR) foam structure, and Evans et al.[39] later coined the term *auxetics* to describe NPR materials.

Auxetic materials are a specific type of material that undergoes expansion when under tension and contraction when under compression, as shown in **Figure 1**.

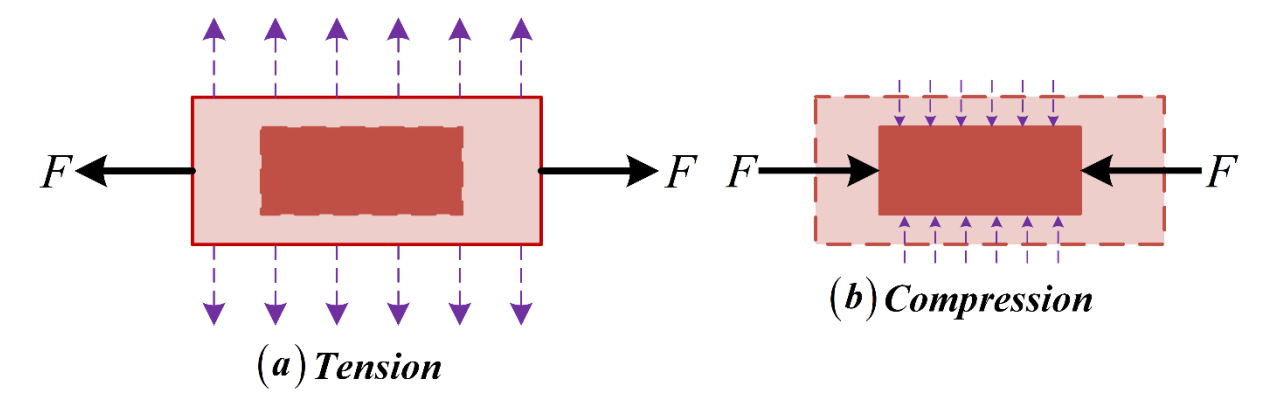


Figure 1. Auxetic material in (a) Tension and (b) Compression.

The unusual behavior of auxetic materials imparts many superior properties to the auxetic material such as improved resistance to shear[40], resistance to indentation [41, 42], resistance to fracture[43], and better energy absorption[44-47]. Topolov[48] conducted simulation-based studies on 1-3 piezo-active composites made from an auxetic polymer matrix and found an improvement in the hydrostatic piezoelectric response of the composite. Krishnaswamy et al.[49] explored polymeric auxetic matrix-based lead-free 0-3 piezocomposites which demonstrated improved mechanical coupling. They studied the effective homogenized electro-elastic properties of auxetic polyethylene matrix and single-crystal BaTiO₃ piezoelectric inclusion-based piezocomposite, where an improvement in the effective properties was observed. This has motivated our work to explore the sensing and energy harvesting capabilities of an auxetic polyethylene matrix-based metamaterial using promising lead-free BCZ-BCT inclusions to create of lead-free piezocomposite material.

In the present work, a polymer-based inherently auxetic material termed polyethylene (PE)[50] was used as a matrix with BCZ-BCT piezoelectric material as an inclusion to prepare a piezocomposite. Effective properties were calculated considering both positive and negative matrix materials at all the volume fractions.

Various approaches have been reported in the literature to calculate the effecting properties like the analytical approach[51, 52], semi-analytical approaches[53, 54], microfield approaches[55-57]. Effective properties can also be calculated by applying the homogenization technique to a representative volume element (RVE) and solving by finite element method and has been extensively reported in the literature[58-63]. In the present study, homogenization technique has been used to calculate effective properties. The calculated effective properties of the composite were used further to study the piezocomposite as sensor and energy harvester. The present study explores BCZ-BCT based 0-3 piezocomposites with both positive and negative Poisson's ratio matrix-based piezocomposite for this purpose.

2. Materials and Methods

The present work explores the sensing and energy harvesting performance of polyethylene matrix-based piezocomposite with BCZ-BCT piezoelectric inclusions. Both negative and positive Poisson's ratio-based polyethylene matrix has been considered in the present study. The polyethylene matrix can be rendered negative or positive Poisson's ratio depending upon how it has been processed and is often referred to as auxetic and non-auxetic metamaterials. Material properties reported in literature Krishnaswamy et al.[49] for the matrix material and Zhang et al.[28] for BCZ-BZT piezoelectric inclusions have been used in the present study. The auxetic and non-auxetic matrix made of polyethylene is assumed to have a Poisson's ratio of -0.32 and 0.2 respectively. The elastic modulus is considered to be $E = 100 \, MPa[49]$. A BCZ-BCT piezoelectric material

was used as an inclusion to form the 0-3 piezocomposite. The piezoelectric material properties are taken from the literature[28, 64, 65] and the elastic material properties are shown in **Figure 2**. Piezoelectric coefficients in transverse and longitudinal modes are $d_{31} = -298 \,\mathrm{pC/N}$ and $d_{33} = 576 \,\mathrm{pC/N}$ and the relative permittivity considered is $\varepsilon_r = 5549$. Six different volume fractions of BCZ-BCT inclusion in polyethylene matrix are considered viz. 4%, 8%, 12%, 16%, 20% and 24%. A cantilever beam structure is used to study the sensing and energy harvesting performance of the material. Structural steel was used as a material for the host cantilever beam having Young's modulus $E = 200 \, GPa$, and density $\rho = 7850 \,\mathrm{kg/m^3}$.

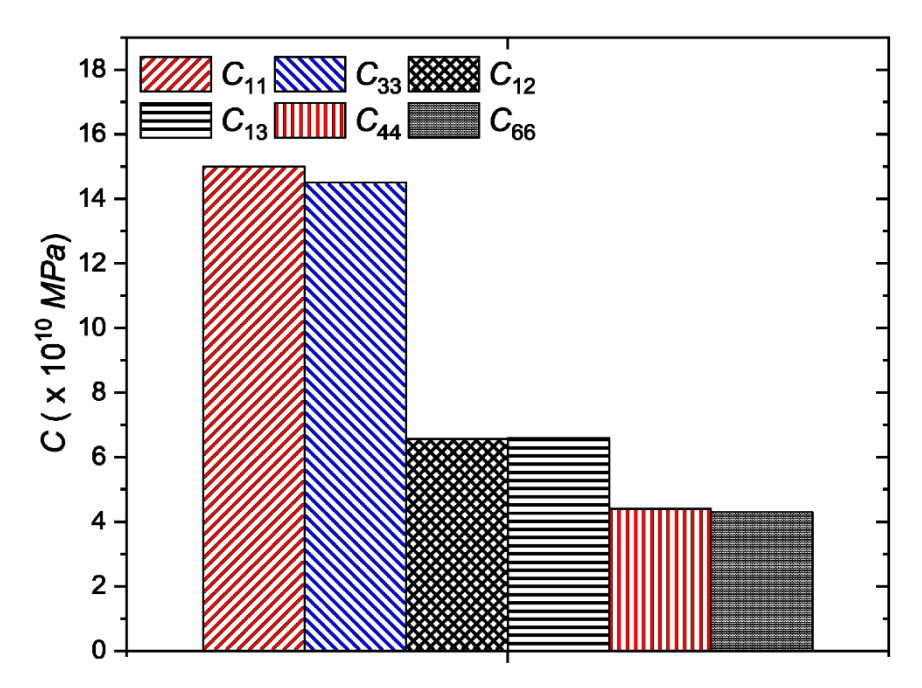


Figure 2. Elastic properties of the BCZ-BCT ceramic.

An extra proof mass $(m_p = 15 \text{ g})$ is attached to the free end to reduce the natural frequency. Acceleration vibration of $1 \times g$ is applied to the base and voltage and power response are collected. The entire structure was subjected to base vibrations in response to which voltage and power are generated and the generated voltage can be used for sensing and the power can be harvested. **Figure 3** shows a schematic diagram of cantilever beam-based piezoelectric energy harvesters, along with their dimensions in millimeters, which are operating in transverse and longitudinal mode.

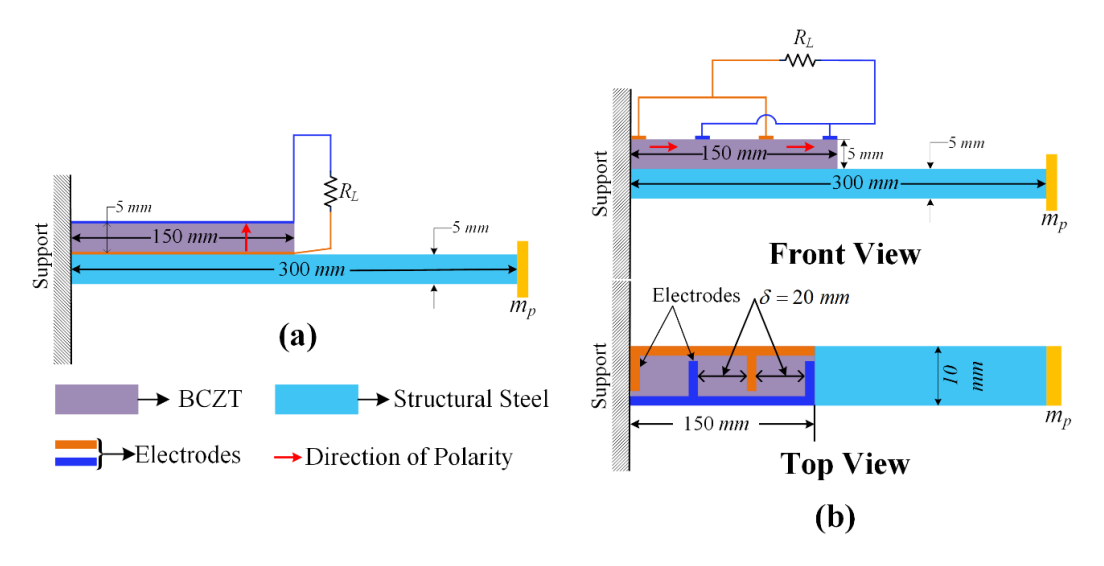


Figure 3. Cantilever beam-based piezoelectric energy harvester operated in (a) Transverse mode and (b) Longitudinal mode (Front and Top View). "BCZ-BCT" in the figure represents 0-3 composite.

Energy is harvested by feeding the piezo-current into an external load (a resistance). Generally, as the load resistance varies, the power that can be harvested also varies and maximum power can be obtained at an optimum resistance $R_L = R_{opt}$. The optimum resistance is inversely related to the capacitance between the electrodes [refer to equation (1)]

$$R_{opt} = \frac{1}{\omega C} \tag{1}$$

where ω is the first natural frequency and \mathcal{C} is the capacitance between the electrodes. Optimum resistance is determined by finding the resistance at which the harvested power becomes maximum.

3. Finite Element Model of the Piezocomposite

The effective elastic and piezoelectric properties of the piezocomposite can be calculated using either the analytical or numerical method[56, 66-68]. Analytical methods are suitable for symmetric geometries but are not suitable for arbitrary or complicated shapes. Numerical methods such as the finite element method (FEM) are more suitable to calculate effective properties for piezocomposites having complex shapes and random distribution of inclusions and have been used by several researchers to calculate the effective properties of piezocomposites[68, 69]. Berger et al.[70] evaluated effective properties using both analytical and numerical methods. Following a similar approach, a unit cell model or a representative volume element (RVE) model is used to calculate the effective properties of the composite. RVE is the smallest region or volume of the composite, which represents a homogeneous medium representing the original composite. The process of replacing the original composite with a homogeneous medium is known as homogenization[71]. A typical RVE containing the inclusions within the matrix is shown in Figure 4.

In the present study, a MATLAB code has been used to generate the RVE. The basic approach was to randomly decide the coordinates of the centers and radii of spheres (which represent the piezoelectric inclusions) which are placed within the unit cell volume of $1 \, \text{m} \times 1 \, \text{m} \times 1 \, \text{m}$ to generate the RVE. As the volume fraction of the RVE increased gradually, the sphere radii were reduced gradually until the final volume fraction is achieved. RVE generated in MATLAB is imported into COMSOL multiphysics to calculate the effective properties.

The BCZ-BCT inclusions are poled in the *z*-direction and the effective elastic and piezoelectric properties of the composite can be calculated using micromechanical analysis[59].

Generating a voltage in response to the applied mechanical stress is referred to as the direct piezoelectric effect and the opposite phenomenon is referred to as the converse piezoelectric effect and constitutes a coupled piezoelectric problem. Electromechanical coupling is considered by taking care of both displacement and electrical degree of freedom. The constitutive equation for the coupled piezoelectric problem in stress-charge form is given by equation (2)[59].

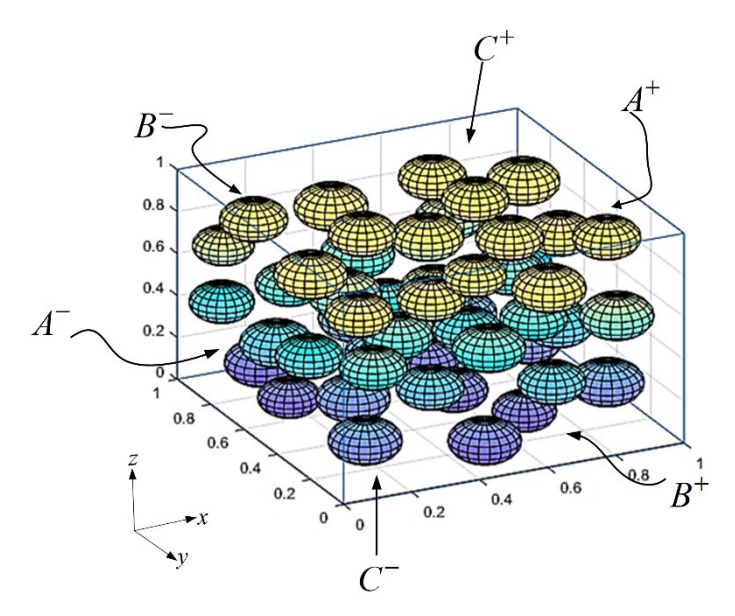


Figure 4. Representative volume element (RVE) containing the piezoelectric inclusions.

The parameters stress T and electrical displacement D to strain S and electric field E are related to each other by material constants C which is the elasticity matrix, ε the permittivity matrix and e the piezoelectric strain coupling matrix. The term e^t refers to the transpose of the coupling matrix.

The piezoelectric material is considered to be a transversely isotropic piezoelectric solid, having a hexagonal crystal symmetry. The number of elastic constants reduces from a total of 21 to 5. Equation (2) in its expanded form is given by equation (3). Only ten material constants are required to describe the behavior of the material given in the equation (3).

In the above equation (3) \bar{T} is the average value of stress, \bar{D} is the average value of the electric displacement, \bar{E} is the average value of the electric field and \bar{S} is the average value of the strain. C, e and ε are the elasticity, piezoelectric strain and permittivity. Perfect bonding is assumed between the polyethylene matrix and the spherical BCZ-BCT piezoelectric particles used as an inclusion.

3.1. Boundary Conditions

Composites can often be represented as a periodic array of RVE's or unit cells. Therefore, responses are simulated using periodic boundary conditions. The application of a periodic boundary condition ensures that the deformation mode remains the same across the RVE and is devoid of interpenetration and separation between the neighboring RVE. Equation (4) gives the boundary condition in terms of Cartesian coordinates[71, 72].

$$u_i = \overline{S}_{ij} x_i + v_i \tag{4}$$

where \bar{S}_{ij} is the average engineering strain, v_i is the global load-dependent local unknown fluctuations. Applying the periodic boundary conditions to the opposite faces of the RVE, the boundary conditions can be written as

$$u_i^{K^+} = \overline{S}_{ij} x_j^{K^+} + v_i^{K^+} \tag{5}$$

$$u_i^{K^-} = \overline{S}_{ij} x_j^{K^-} + v_i^{K^-} \tag{6}$$

In the above equations (5) and (6) K^+ denotes a direction normal to the x plane in the positive direction and K^- denotes a direction normal to the x plane in the negative direction denoted by surface A^- and A^+ in **Figure 4**. Similar boundary conditions may be applied to the opposite surfaces B^-/B^+ and C^-/C^+ .

Table 1. Equations and boundary conditions to calculate effective properties.

Sl. No.	Eff. Coeff.	$A^ (u_i)$	A^+ (u_i)	$B^- \ \left(u_i ight)$	$B^+ \ ig(u_iig)$	$C^- \ (u_i)$	$C^+ \ ig(u_iig)$	Formula
1	\mathcal{C}^{eff}_{11}	0/-	$u_1/-$	0/-	0/-	0/0	0/0	$\overline{T}_{11}/\overline{S}_{11}$
2	\mathcal{C}^{eff}_{12}	0/-	$u_1/-$	0/-	0/-	0/0	0/0	$\bar{T}_{22}/\bar{S}_{11}$
3	\mathcal{C}^{eff}_{13}	0/-	0/-	0/-	0/-	0/0	$u_3/-$	$\overline{T}_{11}/\overline{S}_{33}$
4	\mathcal{C}^{eff}_{33}	0/-	0/-	0/-	0/-	0/0	u_3	$\bar{T}_{33}/\bar{S}_{33}$

5	C_{44}^{eff}	$u_3/0$	$u_3/0$	0/-	0/-	$u_1/-$	$u_1/-$	$\overline{T}_{13}/\overline{S}_{13}$
6	C_{66}^{eff}	$u_2/-$	$u_2/-$	$u_1/-$	$u_1/-$	0/0	0	$\bar{T}_{12}/\bar{S}_{12}$
7	e_{13}^{eff}	0/-	0/-	0/-	0/-	0/0	$0/\Phi$	$-\bar{T}_{11}/\bar{E}_3$
8	e^{eff}_{33}	0/-	0/-	0/-	0/-	0/0	$0/\Phi$	$-\bar{T}_{33}/\bar{E}_3$
9	$e_{15}^{\it eff}$	$u_{3}/0$	$u_3/0$	0/-	0/-	$u_1/-$	$u_1/-$	$ar{D}_1/ar{S}_{31}$
10	$arepsilon_{11}^{eff}$	0/0	$0/\Phi$	0/-	0/-	0/-	0/-	$\overline{D}_1/\overline{E}_1$
11	$arepsilon_{33}^{eff}$	0/-	0/-	0/-	0/-	0/0	0/Φ	\bar{D}_3/\bar{E}_3

The local fluctuations on the two opposite faces are identical, therefore, the applied macroscopic strain can be calculated as,

$$u_i^{K^+} - u_i^{K^-} = \overline{S}_{ij} \left(x_j^{K^+} - x_j^{K^-} \right)$$
 (7) 239

Similarly, for the electric potential, the applied macroscopic electric field is given by,

$$\Phi^{K^{+}} - \Phi^{K^{-}} = \overline{E}_{i} \left(x_{i}^{K^{+}} - x_{i}^{K^{-}} \right)$$
 (8)

The stresses, strains, electrical fields, and electrical displacements are volume average over the entire RVE. The corresponding average values are given by,

$$\overline{S}_{ij} = \frac{1}{V} \int_{V} S_{ij} dV \tag{9}$$

$$\overline{T}_{ij} = \frac{1}{V} \int_{V} T_{ij} dV \tag{10}$$

$$\overline{E}_i = \frac{1}{V} \int_V E_i dV \tag{11}$$

$$\bar{D}_i = \frac{1}{V} \int_V D_i dV \tag{12}$$

In the above equations from (9) to (12), V is the volume of the unit cell. The average properties of the composite are assumed to be the average properties of the unit cell given by equations (9) to (12). The boundary conditions and formulas to calculate different elastic and piezoelectric coefficients are given in **Table 1**. Boundary conditions are applied such that except one all other field components are zero. The effective properties are calculated by finding the ratio of the average values calculated using equations (9) to (12). Effective properties depend upon the inclusions volume fraction, correspondingly a unit cube can be chosen as an RVE.

3.2. Calculation of Stiffness Coefficients

Except for mechanical strain in the first direction, all other strains and electric fields are made zero. Therefore, we have $\bar{S}_{11} \neq 0$, but $\bar{S}_{22} = \bar{S}_{33} = \cdots = \bar{E}_2 = \bar{E}_3 = 0$ [refer to equation (3)]. Applying this, C_{11}^{eff} and C_{12}^{eff} can be calculated using boundary conditions 1 and 2 given in **Table 1**.

$$C_{11}^{eff} = \frac{T_{11}}{\bar{S}_{11}} \tag{13}$$

$$C_{12}^{eff} = \frac{\overline{T}_{22}}{\overline{S}_{11}} \tag{14}$$

Similarly, if $\bar{S}_{33} \neq 0$ but $\bar{S}_{11} = \bar{S}_{22} = \bar{S}_{23} = \dots = \bar{E}_2 = \bar{E}_3 = 0$, then C_{13}^{eff} and C_{33}^{eff} can be calculated using boundary conditions 3 and 4 in **Table 1**.

$$C_{13}^{eff} = \frac{\overline{T}_{11}}{\overline{S}_{33}} \tag{15}$$

$$C_{33}^{eff} = \frac{\overline{T}_{33}}{\overline{S}_{23}}$$
 (16) 267

 C_{44}^{eff} and C_{66}^{eff} are calculated by subjecting the RVE to pure shear conditions. Two pairs of opposite surfaces are constrained to give rise to a pure shear condition as given by conditions 5 and 6 given in **Table 1**. Correspondingly the stiffness coefficients are given by,

$$C_{44}^{eff} = \frac{\overline{T}_{13}}{\overline{S}_{31}} \tag{17}$$

$$C_{66}^{eff} = \frac{\overline{T}_{12}}{\overline{S}_{12}}$$
 (18)

3.3. Calculation of Piezoelectric Coefficients and Dielectric Constants

The effective piezoelectric coefficients e_{13}^{eff} and e_{33}^{eff} and effective value of the dielectric coefficient ε_{33}^{eff} are calculated by applying zero strains on all the opposing faces and by applying an electrical potential gradient along the z direction. In the present case, a unit voltage is applied on the C^+ surface and a zero strain on all the surfaces of the RVE. The effective coefficients are calculated by applying boundary conditions and formulas given by conditions 7, 8, and 11 in **Table 1**. Similarly, the dielectric permittivity ε_{11}^{eff} is calculated by applying unit voltage on the surface A^+ and applying zero strains on all other surfaces. Correspondingly, the boundary condition and formula is given by condition 10 in **Table 1** is used. The effective property e_{15}^{eff} is calculated by applying unit shear strain to opposite faces A^-/A^+ and C^-/C^+ as given by condition 9 in **Table 1**. e_{15}^{eff} can be calculated as,

$$e_{15}^{eff} = \frac{\bar{D}_1}{\bar{S}_{31}} \tag{19}$$

3.4. Finite element model of the Sensor and the Energy Harvester

The finite element method is often used to undertake static and dynamic analysis of piezoelectric-laminated structures[73-77]. A similar approach has been adopted in the present study to calculate the static and dynamic responses. The finite element domain was discretized using shell elements due to their generalized nature[78-80]. Shell elements, being a generalized element, can take care of curvatures in the finite element domain. First-order shear deformation theory was used to formulate the shell element. Since bending stress is maximum at the fixed end in a cantilever beam configuration, the piezoelectric material is attached closer to the fixed end. The cantilever beam and the piezoelectric material were modeled using shell elements. The governing equation of

motion was derived using Hamilton's principle and is given below in equations (20) and (21)[81].

$$\left[M_{uu}^{e} \right] \left\{ \dot{u}^{e} \right\} + \left[C_{uu}^{e} \right] \left\{ \dot{u}^{e} \right\} + \left[K_{uu}^{e} \right] \left\{ u^{e} \right\} + \left[K_{u\varphi}^{e} \right] \left\{ \varphi^{e} \right\} = \left\{ f_{ext}^{e} \right\}$$
(20)

$$\left[K_{\varphi u}^{e}\right]\left\{u^{e}\right\} + \left[K_{\varphi\varphi}^{e}\right]\left\{\varphi^{e}\right\} = \left\{Q^{e}\right\}$$
(21) 300

In equations (20) M^e_{uu} , C^e_{uu} and K^e_{uu} are the consistent mass, damping and stiffness matrix for an element. $K^e_{u\varphi}$ and $K^e_{\varphi u}$ are the coupling matrices for an element. $K^e_{\varphi \varphi}$ dielectric stiffness matrix for an element. The nodal field variables record the response in terms of displacement $\{u^e\}$ and potential $\{\varphi^e\}$ at the element. The external force and charges on a single element are given by $\{f^e_{ext}\}$ and $\{Q^e\}$.

Equation (22) gives the elemental stiffness matrix.

$$\begin{bmatrix} K \end{bmatrix}_e = \begin{bmatrix} K_{uu}^e & K_{u\varphi}^e \\ K_{\varphi u}^e & K_{\varphi\varphi}^e \end{bmatrix}$$
 (22) 307

Global equations, obtained by assembling the elemental equations, are given below in equations (23) and (24).

$$[M_{uu}]\{\ddot{u}\} + [C_{uu}]\{\dot{u}\} + [K_{uu}]\{u\} + [K_{u\varphi}]\{\varphi\} = \{f^{ext}\}$$
(23)

Matrices in equations (23) and (24) are corresponding global matrices obtained after assembly. Equations (23) and (24) are coupled together to achieve the final coupled global equation, as given below in equation (25)

$$\begin{bmatrix} M_{uu} & 0 \\ 0 & 0 \end{bmatrix} \begin{cases} \ddot{u} \\ \ddot{\varphi} \end{cases} + \begin{bmatrix} C_{uu} & 0 \\ 0 & 0 \end{bmatrix} \begin{cases} \dot{u} \\ \dot{\varphi} \end{cases} + \begin{bmatrix} K_{uu} & K_{u\varphi} \\ K_{\varphi u} & K_{\varphi \varphi} \end{bmatrix} \begin{Bmatrix} u \\ \varphi \end{Bmatrix} = \begin{cases} f^{ext} \\ Q \end{cases}$$
(25) 315

A Dirichlet boundary condition (u = 0) is applied at the fixed end. Initial values of the displacement and charge distribution are considered to be zero. The system is considered to have zero initial displacements and charge. The system response, measured in terms of open-circuit voltage, is given by equation (26). Correspondingly harvested power can be calculated by calculating current and voltage across the resistance using equations (27) to (30).

$$\{\varphi\} = -\left[K_{\varphi\varphi}\right]^{-1}\left[K_{\varphi u}\right]\{u\} \tag{26}$$

Current can be calculated from accumulated charge and voltage developed given below in the following equations,

$$i = -\frac{dQ}{dt} \tag{27}$$

$$i = \frac{V}{R_L} \tag{28}$$

Using the expression of charge from equation (24) and equation (27), the current is given by,

$$i = -\frac{dQ}{dt} = -\frac{d}{dt} \left(\left[K_{\varphi u} \right] \left\{ u \right\} + \left[K_{\varphi \varphi} \right] \left\{ \varphi \right\} \right) \tag{29}$$

Using equations (28) and (29), the voltage is given by,

$$V = R_L \times -\frac{d}{dt} \left(\left[K_{\varphi u} \right] \left\{ u \right\} + \left[K_{\varphi \varphi} \right] \left\{ \varphi \right\} \right) \tag{30}$$

The power across the load resistance can be calculated using equations (29) and (30) using the relation P = Vi. For a much detailed formulation, refer to the authors other paper [82].

4. Results and Discussion

As the inclusion volume fraction increased, the effective properties improved which in turn increased the sensing voltage and harvested power. The same study was repeated at 24% volume fraction for a range of Poisson's ratio ($\nu = -0.9$ to 0.4). Effective properties, sensing voltage, and harvested power all showed significant improvement in the case of the auxetic matrix at the negative extreme of the Poisson's ratio spectrum compared to the positive one.

The effective stiffness parameters of the piezocomposite with auxetic and non-auxetic matrices at different volume fractions are shown in **Figure 5**. Mixture rule and higher stiffness of inclusions explain the increase in stiffness of piezocomposite with volume fraction. A similar pattern can be observed in the case of effective piezoelectric properties e_{31}^{eff} and e_{33}^{eff} , as shown in **Figure 6** and is also explained by the rule of mixtures.

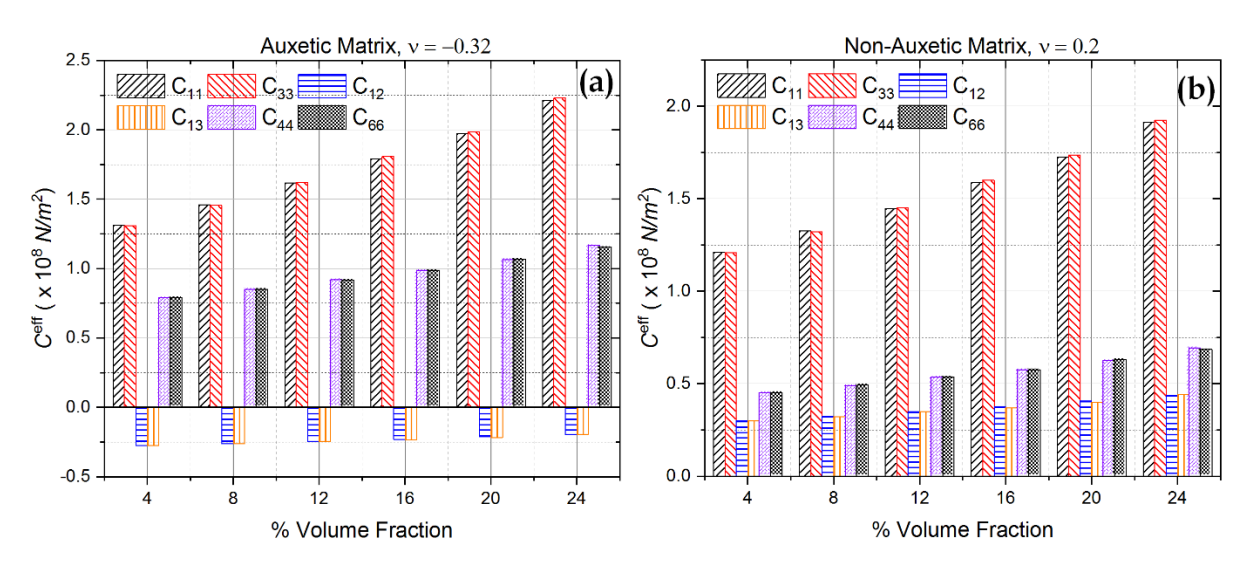


Figure 5. Effective stiffness parameters calculated at different volume fractions (a) Auxetic matrix (b) Non-Auxetic Matrix.

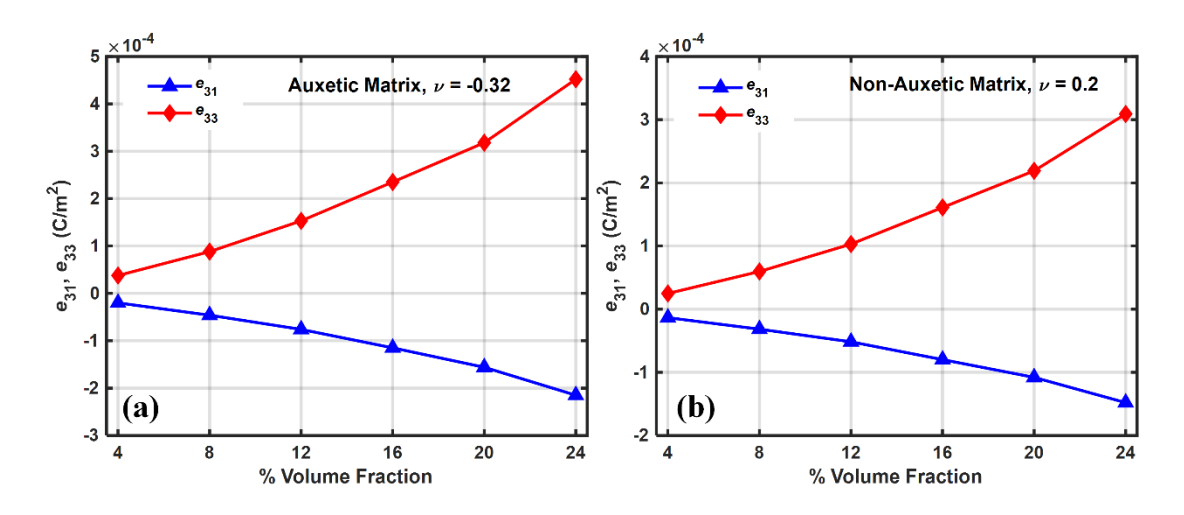


Figure 6. Plot of effective piezoelectric coefficients vs. volume fraction for (a) Auxetic material (b) Non-Auxetic material.

The Poisson's ratio was found to have an insignificant effect on the relative permittivity (ε_s measured at constant strain) of the piezocomposite material; this is to be expected since the stress and stiffness terms are not involved in the determination of the effective permittivity.

The relative permittivity is calculated using the boundary conditions 10 and 11 given in **Table 1**. Neither the stress terms \bar{T}_{ij} and nor the stiffness coefficients C_{ij}^{eff} are involved in the calculation of the effective relative permittivity. This means that Poisson's ratio affects only the stiffness parameters and not the electric field (\bar{E}_1) and the electric displacement $(\bar{D}_1)[83]$, which explains why Poisson's ratio has an insignificant effect on the relative permittivity of the piezocomposite. Sensing and energy harvesting was carried out both in transverse mode $(d_{31} \mod e)$ and longitudinal mode $(d_{33} \mod e)$. The cantilever beam-based energy harvester operating in the above two modes was subjected to a base vibration and the responses were collected in the frequency domain. **Figure 7** shows the frequency domain plot of the open-circuit voltage, namely the sensing capability, obtained from piezocomposites at different volume fractions of BCZ-BCT in the frequency domain. **Figure 8** shows the maximum values of the open circuit voltage, or sensing voltage, at different volume fractions.

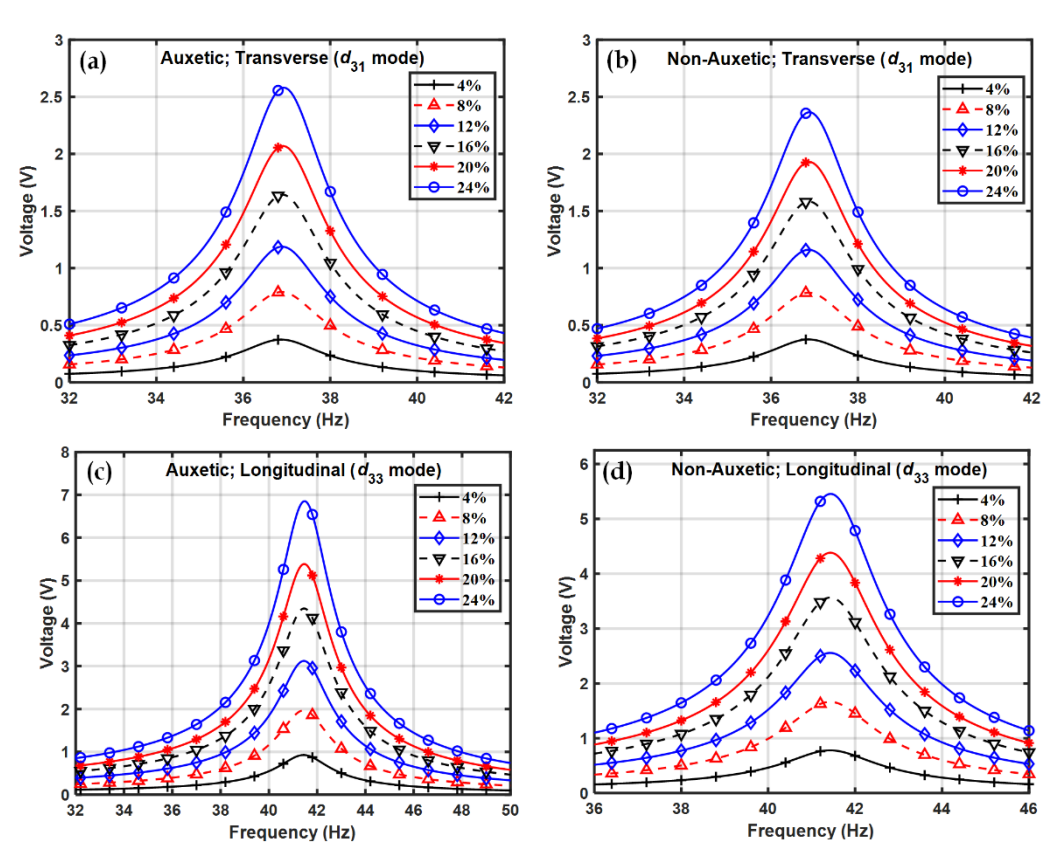


Figure 7. Voltage obtained from piezocomposite in the frequency domain at different volume fractions of BCZ-BCT in transverse (d_{31}) mode for (a) Auxetic, (b) Non-Auxetic piezocomposite and in longitudinal (d_{33}) mode of (c) Auxetic and (d) Non-Auxetic piezocomposite.

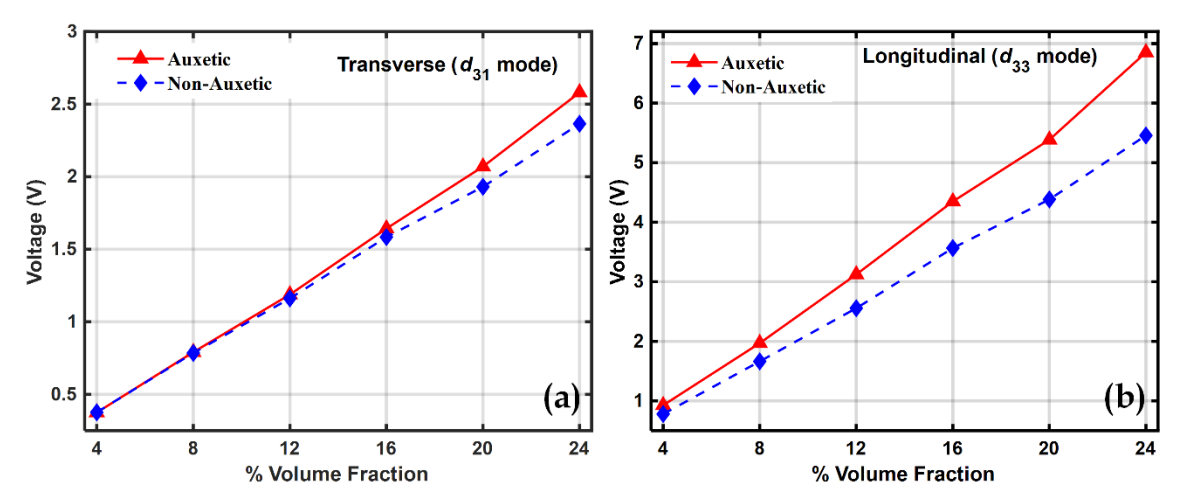


Figure 8. Maximum voltage at different volume fractions of BCZ-BCT in (a) transverse (d_{31}) mode and (b)

longitudinal
$$(d_{33})$$
 mode

The open-circuit voltage for both the piezocomposites are shown operating both at d_{31} and d_{33} mode. The sensing voltage was found to increase with an increase in the volume fraction of the piezoelectric material and this can be explained by the fact that as the volume fraction increases, the piezoelectric coefficients also increase with the volume fraction, as shown in **Figure 6**. Compared to non-auxetic, a significant improvement in sensing voltage was observed in auxetic piezocomposite. In the transverse and longitudinal configuration, the auxetic piezocomposite reported 2.4 and 1.4 times more sensing voltage than the non-auxetic one.

At 24% volume fraction.

It can also be observed that voltage in d_{33} mode is much higher than the voltage in d_{31} mode. The electrode arrangement in the transverse and longitudinal configuration are Top Bottom Electrode (TBE) and interdigitated electrodes respectively. It has been observed that the capacitance in the longitudinal d_{33} mode is always lower than that in transverse d_{31} mode and this could be the reason why the open-circuit voltage is higher in longitudinal (d_{33}) mode compared to that in transverse (d_{31}) mode[84]; since the relationship between charge, voltage and capacitance is given by Q = CV.

The energy harvesting performance is studied by connecting the harvester to an external load, in the form of a resistance R_L . The maximum power is harvested at the optimum resistance of the load resistance, which depends upon the natural frequency ω of the structure and the capacitance C between the electrodes, given by equation (31).

$$R = \frac{1}{\omega C} \tag{31}$$

A power vs. resistance graph is used to estimate the optimum resistance R_{opt} at which maximum power is obtained. **Figure 9** shows the plot of the power vs resistance for both auxetic and non-auxetic matrix-based piezocomposites operating in both the modes, transverse and longitudinal. The harvester and the external load form a RC circuit. Since the capacitance of the piezoelectric material does not change by varying the external load resistance it is possible to determine the optimum resistance at which power attains its maximum value which is evident in the plots shown in **Figure 9**. The optimum resistance generally depends upon the natural frequency of vibration ω of the structure. It can be observed that as the volume fraction of inclusions increases, the harvested power also increases. This is obvious and can be explained by the mixture rule since there are more piezoelectric inclusions present in the composite. It can also be observed that as the volume fraction of inclusion changes, the optimum resistance also

changes. This is because with a change in the volume fraction of inclusions both the stiffness and capacitance of the piezocomposite will change; for example, the increase in permittivity and therefore capacitance with increasing inclusion fraction will lead to a reduction in optimum resistance from equation (31). The change in stiffness will also affect the natural frequency of vibration of the structure. These factors lead to the observation that as the volume fraction of inclusion changes, the optimum resistance at which maximum power is obtained also changes (as given in equation (31)).

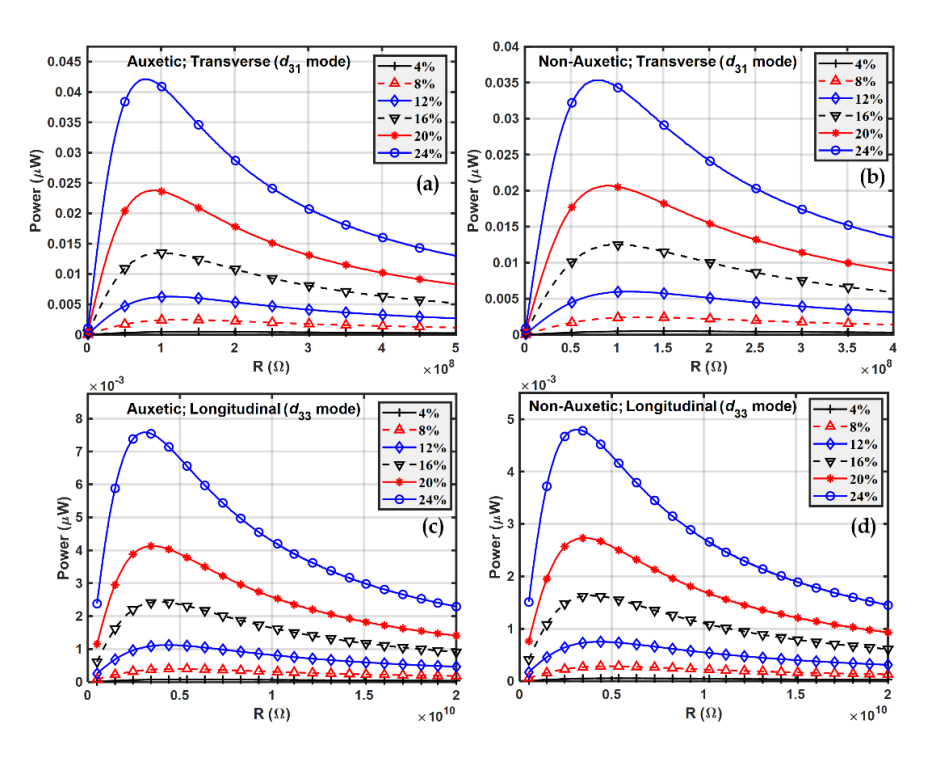


Figure 9. Power vs Resistance at different volume fractions of BCZ-BCT in transverse d_{31} mode of (a) Auxetic (b) Non-Auxetic; and in longitudinal (d_{33}) mode (c) Auxetic (d) Non-Auxetic

The optimum resistance R_{opt} is obtained from **Figure 9** for the different cases shown and **Figure 10** shows how maximum power varies with frequency at the optimum

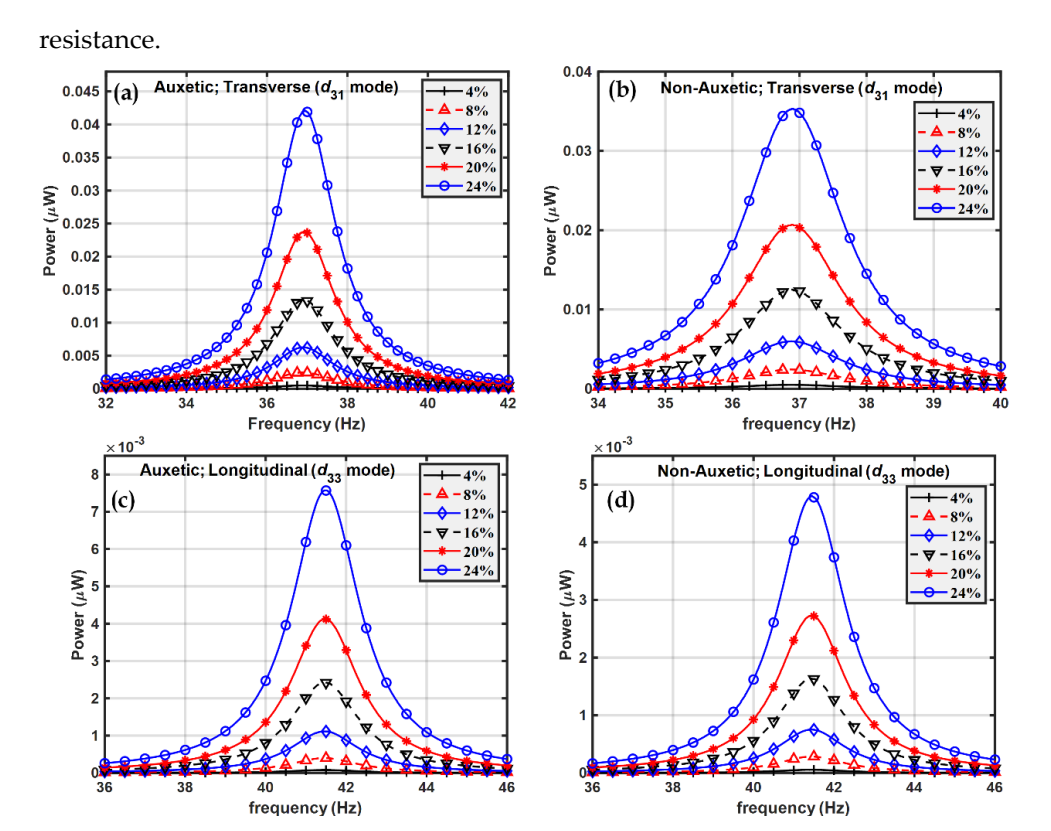


Figure 10. Power in the frequency domain at different volume fractions of BCZ-BCT in transverse (d_{31}) mode for (a) Auxetic and (b) Non-auxetic piezocomposite; and in longitudinal (d_{33}) mode for (c) auxetic and (d) non-auxetic piezocomposite

The natural frequency of vibration was not found to vary significantly in the frequency domain plots in **Figure 7** and **10.** A possible explanation is that the elastic properties of the host steel beam structure dominate and piezoelectric properties have little effect on the natural frequency of vibration of the structure.

As a result, the natural frequency of vibration remains almost the same in both the piezocomposites, auxetic and non-auxetic. From **Figure 9**, **10**, and **11** it can be observed that as the volume fraction of inclusions increases, the maximum power also increases and this can be explained by the rule of mixtures and increased piezoelectric coefficients. Auxetic materials showed a marked increase in harvested power, compared to their non-auxetic counterpart in both the modes of operation, transverse (d_{31}) and longitudinal (d_{33}). The auxetic piezocomposite showed an increase in power by approximately 19% in the transverse mode and approximately 58% in the longitudinal mode at a volume fraction of 24%. The figure of merits (FOM) is calculated to validate the harvested power, where the FOM of the energy harvester is given by equation (32)[85]

$$FOM = \frac{d^2 \times E}{\varepsilon} \tag{32}$$

where d is the piezoelectric coefficient, E is Young's modulus and E is the dielectric permittivity. **Figure 12** shows the figures of merit calculated at different volume fractions. Comparative analysis of **Figure 11** and **12** explain the pattern of the rise of maximum power with volume fraction.

At higher volume fractions the effective properties increase. However, their relative rate of increase decides the nature of the FOM graph. The faster rate of increase in the numerator compared to the denominator in equation (32) explains why FOM increases as the volume fraction rises. Correspondingly, the maximum power increases accordingly.

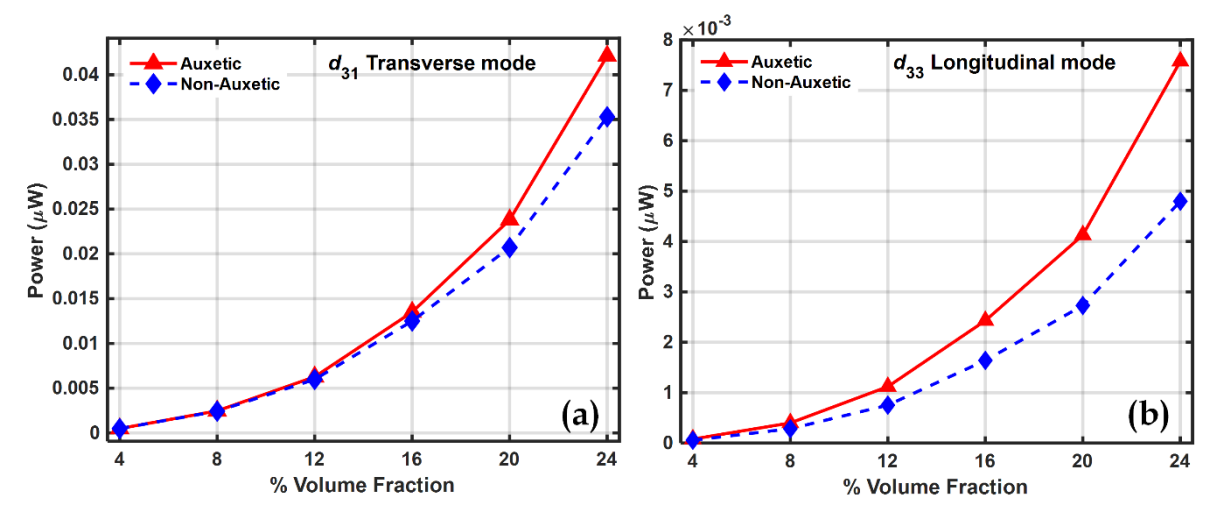


Figure 11. Maximum power vs volume fraction of BCZ-BCT auxetic and non-auxetic piezocomposite in (a) Transverse mode (b) Longitudinal mode.

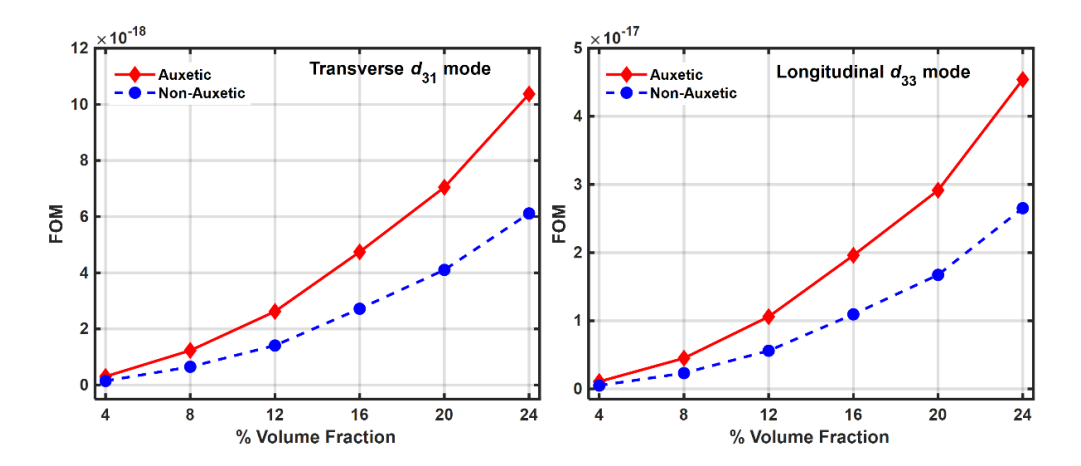


Figure 12. Variation of FOM with volume fraction for both Auxetic and Non-Auxetic materials in (a) Transverse (d_{31}) mode and (b) Longitudinal (d_{33}) mode

To explore further the effect of Poisson's ratio on the energy, the Poisson's ratio is varied theoretically between -0.9 to 0.4. Negative Poisson's ratio, as large as $\nu = -0.9$, has been mentioned[86, 87]. The effective elastic/stiffness and piezoelectric properties at 24% volume fraction is calculated as shown in **Figure 13** (a) to (d).

Figure 14(a) shows the variation of sensing voltage with Poisson's ratio in both the modes, d_{31} and d_{33} modes. Larger voltage in transverse mode could be because this configuration has a larger capacitance than the longitudinal mode[84].

In d_{31} configuration, the voltage increased by approximately 4 times and in the longitudinal mode, it is increased by approximately 5.6 times. Assuming that the external loads will remain constant when the beam is subjected to base vibrations, the deflection will depend upon the stiffness/elastic properties shown in **Figure 13** (a) to (c). The sensing voltage pattern is shown in **Figure 14**(a) and is due to the cumulative effect of all these properties.

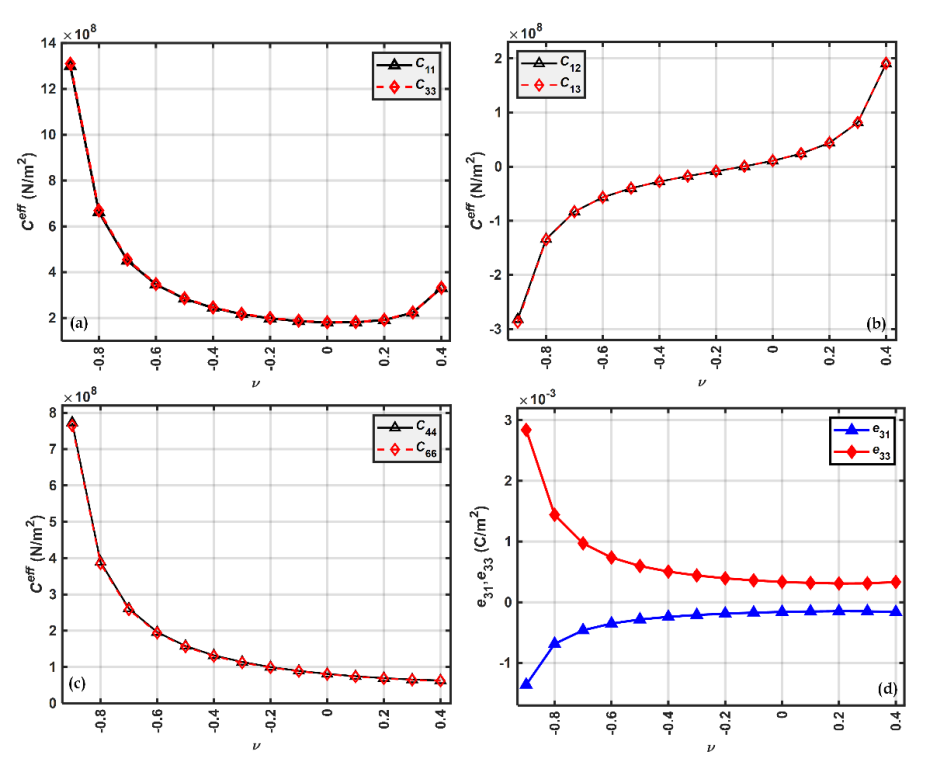


Figure 13. Effective stiffness and piezoelectric properties variation with Poisson's ratios (a) C_{11} , C_{22} (b) C_{12} , C_{13} (c) C_{44} , C_{66} and (d) e_{31} , e_{33}

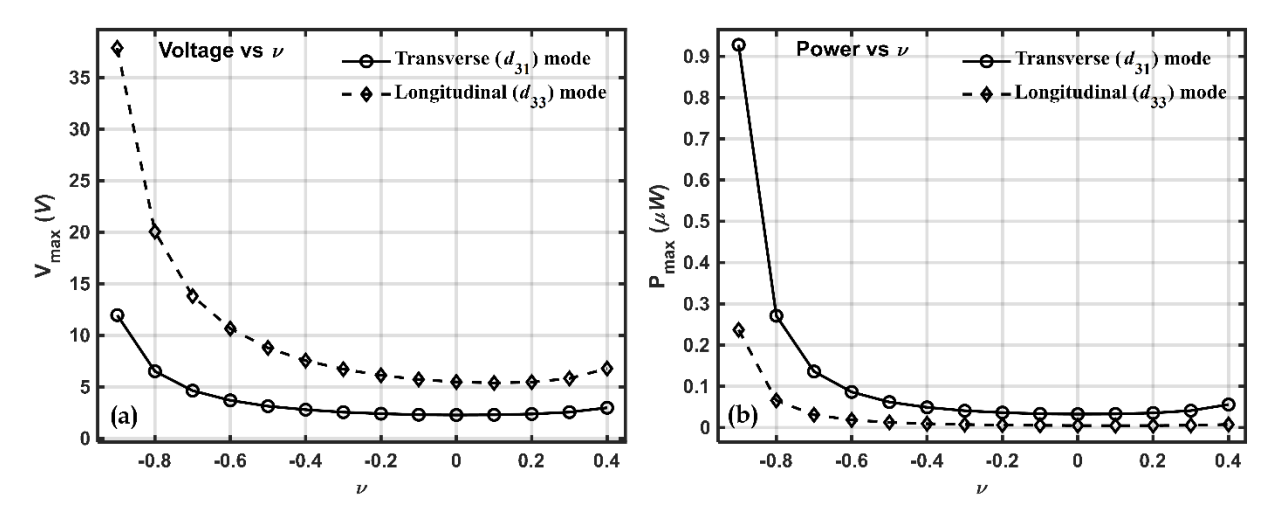


Figure 14. Plot of (a) maximum voltage and (b) maximum power w.r.t Poisson's ratio in Transverse (d_{31}) and Longitudinal (d_{33}) mode. Figure 14(b) shows the variation of power harvested at optimum resistance with Poisson's ratio in the two modes of operation, transverse and longitudinal.

In the transverse mode (\bar{d}_{31}) the auxetic piezocomposite at $\nu = -0.9$ generated approximately 16% more power than the non-auxetic piezocomposite at $\nu = 0.4$. The corresponding increase in the longitudinal mode (d_{33}) is ~ 32%. Larger capacitance in transverse (d_{31}) mode leads to accumulation of more charges and hence more current in d_{31} configuration compared to that in d_{33} configuration. This is due to the accumulation of more charges and current in the d_{31} configuration than in the d_{33} configuration.

× 10⁻¹⁷

Since power depends upon the square of the current term i.e., $P = i^2 R_L$, therefore, d_{31} configuration gives higher power than d_{33} . This can also be explained by the relative variation of material properties with volume fractions as can be observed from the similarity in FOM (equation (32)) and harvested power plots with Poisson's ratio as shown in **Figure 14**(b) and **15**. The difference in magnitude trends between FOM and harvested energy is due to the FOM providing a purely material-based and geometry independent comparison, while the harvesting device models exhibiting different effective areas and electrode spacings in the d_{33} and d_{31} mode[84, 85, 88, 89].

-0.4

-0.2

-0.8

Figure 15. FOM vs ν (a) Transverse (d_{31}) mode and (b) Longitudinal (d_{33})mode.

Transverse mode

-0.4

-0.2

494

486

487

488

489

490

491

492

493

495496

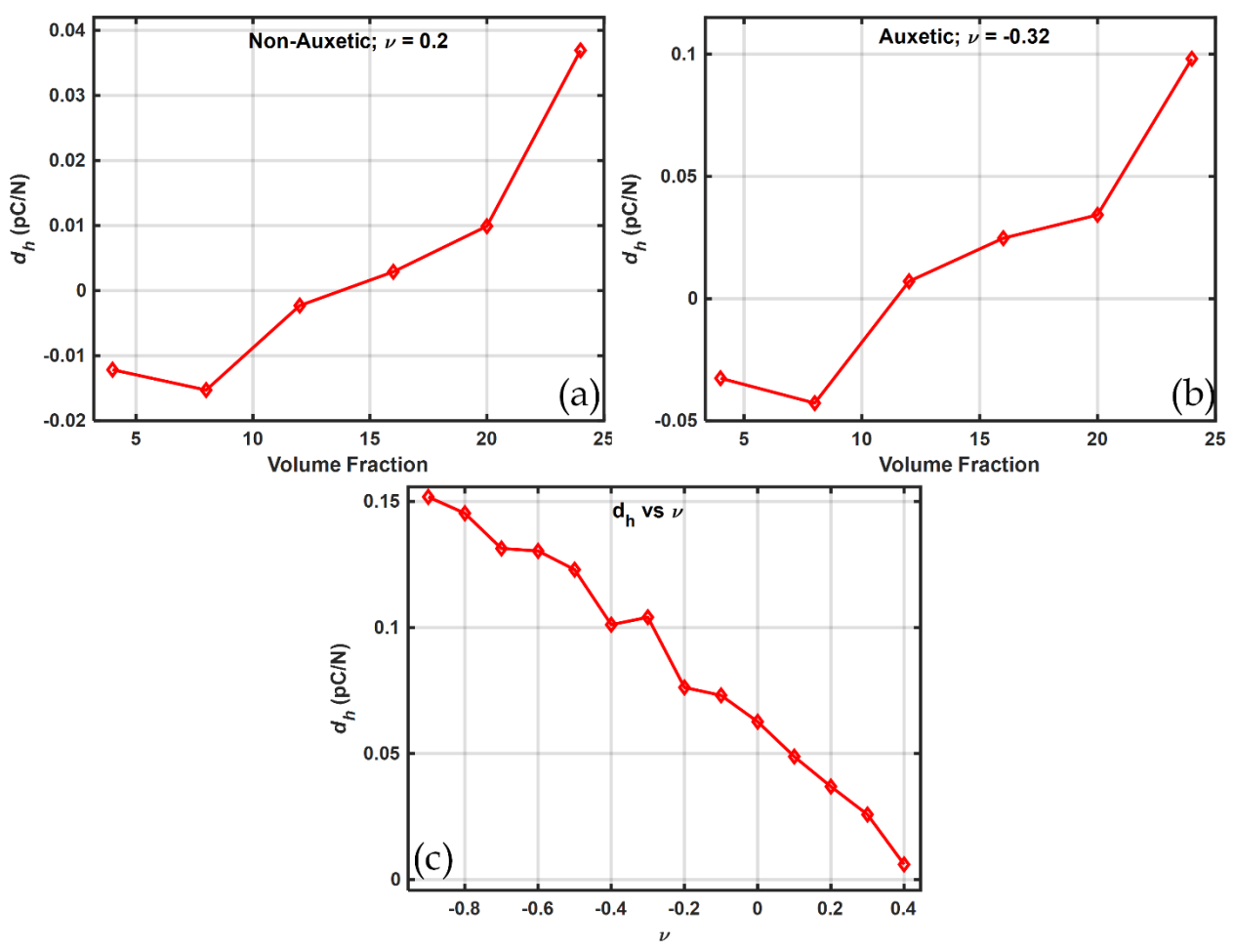


Figure 16. Hydrostatic charge coefficient d_h calculated for (a) Non-Auxetic, (b) Auxetic piezocomposite and, (c) in the Poisson's ratio range of -0.9 to 0.4.

Figure 16 shows the hydrostatic charge coefficient at different volume fractions (Figure 16(a) and (b)) and at different Poisson's ratios (Figure 16 (c)) at a volume fraction of 24%. The hydrostatic charge coefficient is calculated using the relation (33).

$$d_b = 2d_{31} + d_{33} \tag{33}$$

It can be observed from Figure 16 (a) and (b) that hydrostatic coefficient first decreases and then increases with an increase in the volume fraction of the inclusions within the matrix. It can be observed from Figure 16(a) and (b) that the hydrostatic charge coefficient increase with an increase in volume fraction of the inclusions and is explained by the mixture rule. However, the use of auxetic matrix significantly improved the hydrostatic charge coefficient d_h . This is further confirmed by Figure 16(c) where the maximum value of the hydrostatic coefficient is observed at the negative end of the Poisson's ratio spectrum at $\nu = -0.9$. The improved and superior performance of the auxetic piezocomposite over the non-auxetic one could be due to more effective strain transfer to the piezoelectric inclusions in the case of auxetic piezocomposite than in the non-auxetic. This is due to the superior mechanical coupling of the strain applied to the rigid BCZ-BCT piezoelectric inclusions embedded in the soft polyethylene matrix [49, 90].

Table 2 lists the previous works related to auxetic composites and piezocomposites and corresponding improvements achieved. Achievement in the present work in comparison to the previous is also presented.

Table 2: Previous work done on Auxetic materials.

		Table 2. I levious work	done of	ii 71uxetie materia	
S1.	Literature	Auxetic Type	- $ u_{min}$	Study Type	Improvements/
No.		(Structure/Material)	min	Study Type	Achievements
				Experimental	Improved
1.	Lakes[87]	NPR Auxetic foam	-1.0		resilience &
					toughness
				Analytical/	Laminate
2	M:1:1041	Laminated Fibrous	0.07	Experimental	orientation &
2.	Miki[91]	Composite	-0.37		NPR
					Correlation
		I (I NDD		Analytical/	Isotropic
2	1 611. 5001	Isotropic NPR,	4	Mathematical	materials with
3.	Milton[92]	Structure based/Two	-1	Model	$\nu = -1$
		phase composites.			achieved
					Enhanced
	Nkansah	Fibre reinforced		Numerical	transverse
4.	[93]	composite with	-0.9	study (FEM)	modulus of the
		NPR.			composite
		Auxetic Composites	-0.16	Experimental	Enhanced
5.	Alderson	•		Studies	mechanical
	[94]				properties
6.	Alderson	Auxetic		Experimental	Improved
	[50, 95]	Polyethylene Matrix		Studies	flexural
		, ,			properties,
			-0.32		large
					indentation
					resistance.
7.	Subramani	Auxetic structure	-5.20	Analytical	High
	[96]	composites		model/	strength/High
		1		Experimental	energy
				•	absorption
					capacity
8.	Krishnasw	Inherently and		Numerical/	Improved
	amy et	designed structures		Experimental	piezoelectric
	al.[49]	auxetic	-0.32	Study	Properties
	. ,	piezocomposite		,	1
9.	Karmakar	KNNNS-BNZH		Numerical/	Improved
	et al.[82]	auxetic polyethylene	-0.9	FEM	sensing and

521

520

		based			energy
		piezocomposite			harvesting
10.	Present	BCT-BZT auxetic		Numerical/	performance
	Work	polyethylene based	-0.9	FEM	
		piezocomposite			

5. Assumptions and Limitations

Finite element analysis-based comparative study was conducted to study auxetic and non-auxetic piezocomposite for sensing and energy harvesting applications.

Finite element method is a popular approximate solution method that provides solutions to many practical engineering problems. However, this study is based on certain assumptions which limit the scope of the study. Those assumptions and limitations should therefore be kept in mind while implementing this kind of model. A unit cell model, where the RVE is assumed to be a unit cube, has been used to predict the effective properties of the piezocomposite. The above model assumes that the properties of the entire material represent the average property of the unit cell as a whole. In addition, this model assumes that the effective properties depend on the volume fraction of the inclusion and not on the particle size of the inclusions. Therefore, this model is to be used in those cases where there is a uniform and homogeneous distribution of inclusions within the matrix volume. In addition, care should be taken that the present model only considers the volume fraction of the inclusion and not their size within the RVE. The ambient base vibration to which the beam is subjected is assumed to be very small so that the body loads acting on the beam are assumed to be in the reign of linear piezoelectricity, and not non-linear effects associated with domain motion. The model will not be able to predict other important phenomena and parameters such as electrical breakdown strength, fatigue life, and life cycle of the cantilever beam-based energy harvester.

6. Conclusion

Finite element analysis was carried out on 0-3 polyethylene and BCZ-BCT based piezocomposite materials to determine the effective properties of the piezocomposite using a homogenization technique. An RVE having unit dimensions, also called a unit cell, is defined, and periodic boundary condition is applied to calculate the effective properties at six different volume fractions (4%, 8%, ..., 24%). The harvester performance is evaluated in terms of sensing voltage and harvested power using the calculated values of the effective properties. Improved performance was observed at higher volume fractions and can be explained by the rule of mixtures. An overall performance improvement was observed in auxetic piezocomposite compared to non-auxetic. This is because the strain is transferred to the inclusions in a much better way in the case of the auxetic matrix compared to non-auxetic matrix due to improved mechanical coupling. At a 24% volume fraction, the auxetic piezocomposite ($\nu = -0.32$) generated 8% and 25.5% more sensing voltage in transverse and longitudinal modes respectively compared to its non-auxetic counterpart ($\nu = 0.2$). A corresponding increase in harvested power is approximately 20% and 58% in transverse and longitudinal mode respectively.

Sensing voltage and power were calculated at 24% volume fraction for a range of Poisson's ratio between -0.9 to 0.4. Sensing voltage and the harvested power increased significantly at the negative extreme of the Poisson's ratio spectrum when Poisson's ratio is -0.9. Compared to non-auxetic, the auxetic piezocomposite generated 4 and 15.5 times more sensing voltage and power in d_{31} configuration. Corresponding increment in the d_{33} configuration was about 5.6 and 34 times respectively. The above studies conclude that piezocomposites made of negative Poisson's ratio metamaterial can significantly improve the voltage and power output of the harvester.

Conflicts of Interest: - The authors declare that they have no known competing financial interests or personal relationships that could have appeared to influence the work reported in this paper.

Acknowledgments: This work was supported by Researchers Supporting Project number (RSP-2021/100), King Saud University, Riyadh, Saudi Arabia. The authors would like to thank the Innovative Research and Management Centre (iRMC), Universiti Tenaga Nasional, Malaysia for providing research publication BOLD grant (J510050002) and UNITEN R&D Sdn Bhd Seed Fund (U-TV-RD-20-10).

Annexure

The finite element model used in the present work is validated by comparing the effective properties of piezoelectric fibers (PZT-5) embedded in a polymer matrix by Finite Element Method (FEM) and Asymptotic Homogenization Method (AHM) by Berger et al.[60]. The results obtained by the present FEM method were found to be in good agreement with FEM and AHM method reported in Berger et al.[60].

Figure 17, 18 and 19 compare the effective properties calculated by the present FEM method and by Berger et al.[60]. The present FEM model for the piezoelectric energy harvester is validated by comparing the voltage generated per unit base acceleration for a PZT-5A piezoelectric material attached to a host structure, as given in Erturk and Inman[97]. The parameters of the piezoelectric material and the host beam, taken from Erturk and Inman[97] are given in Table 3. Figure 20 shows a comparison plot of voltage calculated per unit base acceleration by the present FEM method and by Erturk and Inman[97]. It can be observed that voltage calculated per unit base acceleration calculated by Erturk and by present FEM almost matches with each other, hence validating the present FEM model.

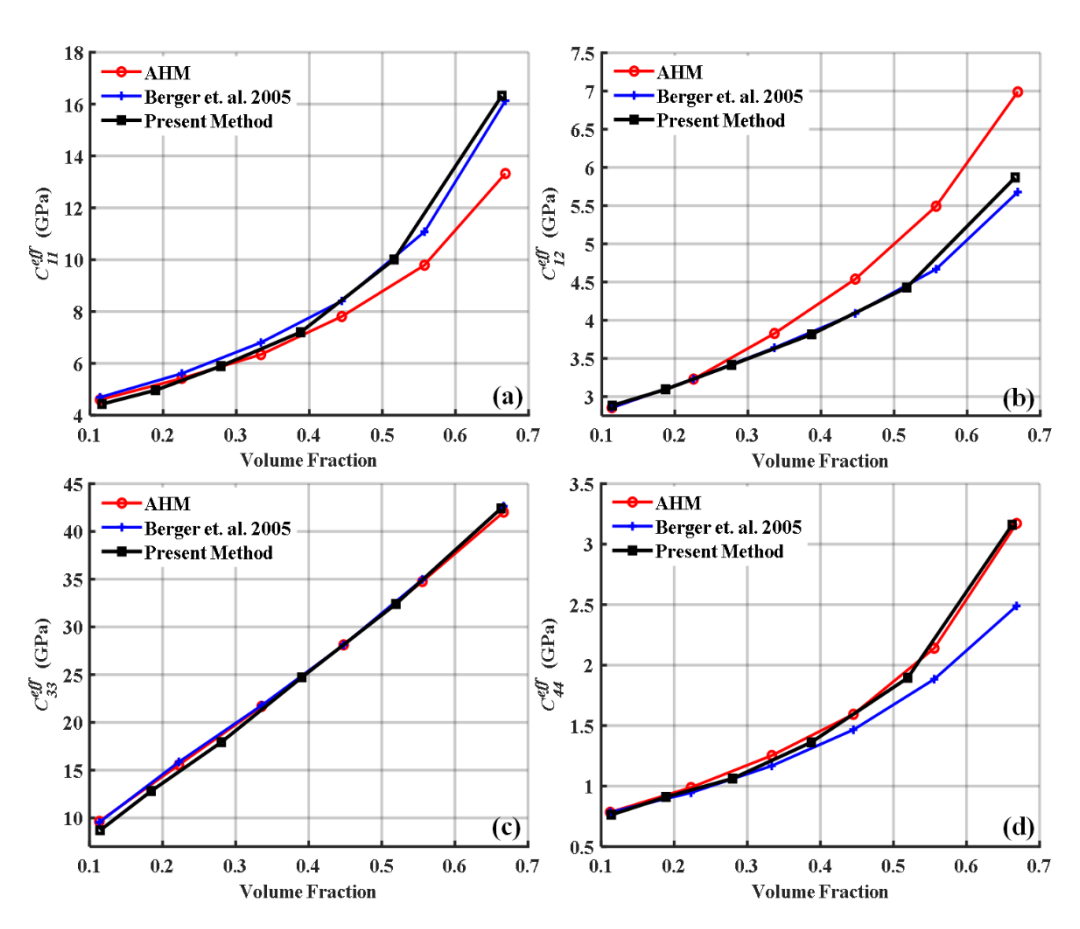


Figure 17. Validation of present model by comparing effective stiffness properties

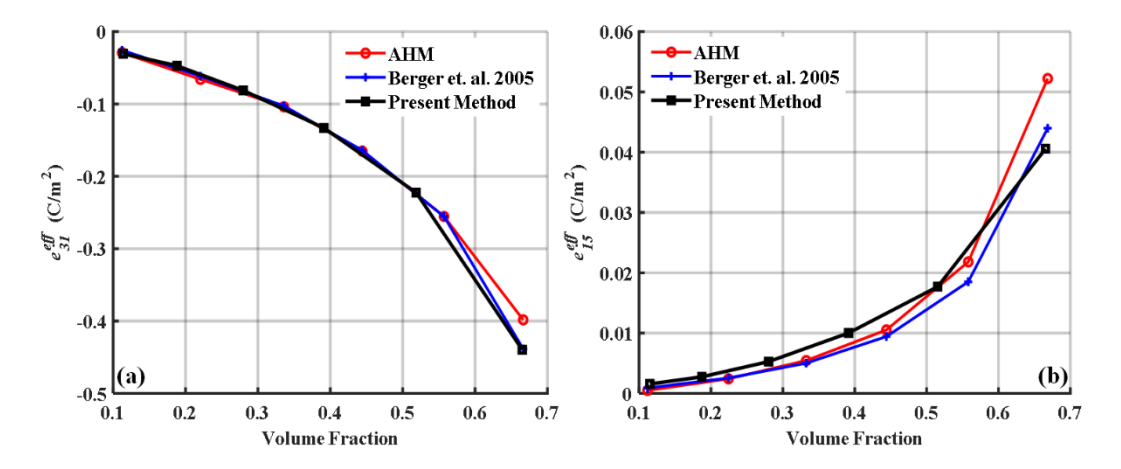


Figure 18. Validation of the present model by comparing the effective piezoelectric properties.

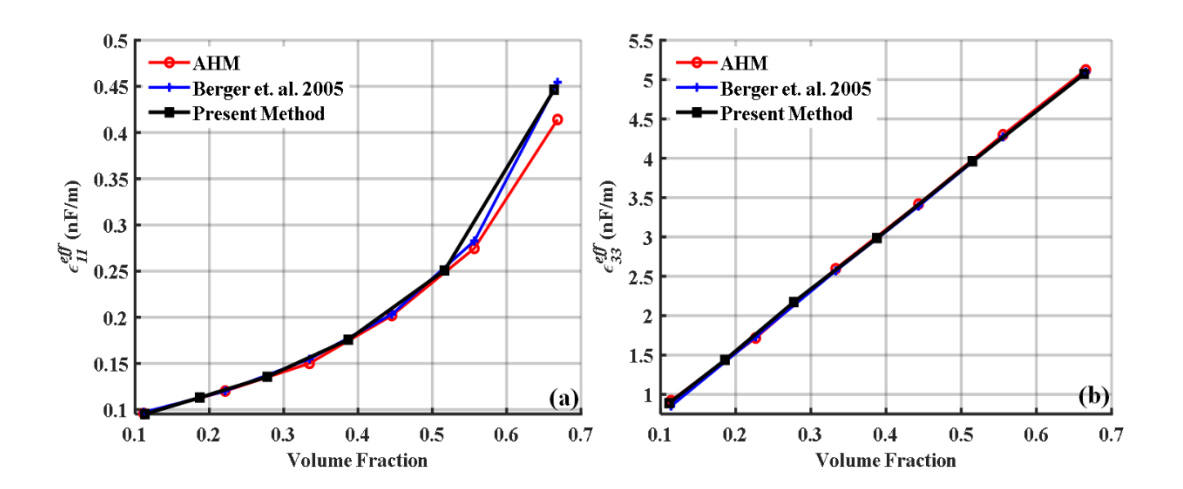


Figure 19. Validation of present model by comparing effective relative permittivity.

Table 3: Material properties of host beam and piezoelectric patch for validating the energy harvester model

1 1	1 0 03		
Piezoelectric Material Properties	Host Material		
(PZT-5A)	(Metal Beam)		
$C_{11}^E = C_{22}^E = 120.3 \ GPa$	Young's Modulus $E = 100 GPa$		
$C_{33}^{E} = 110.9 GPa$ $C_{12}^{E} = 75.2 GPa$	Mass Density = $\rho = 7165 kg/m^3$		
$C_{13}^E = C_{23}^E = 75.1 GPa$	Poisson's ratio = $\nu = 0.3$		
$C_{66}^{E} = 22.7 GPa$	Rayleigh Coefficients		
$e_{31}^{E} = e_{32}^{E} = -5.2 (C/m^{2})$ $e_{33}^{E} = 15.9 (C/m^{2})$	$\alpha = 4.886 rad/s$		
Mass Density = $\rho = 7800 \ kg/m^3$	$\beta = 1.2433 \times 10^{-5} (s/rad)$		
Permittivity = $\epsilon_r = 15.94 (nF/m)$			

592

593594

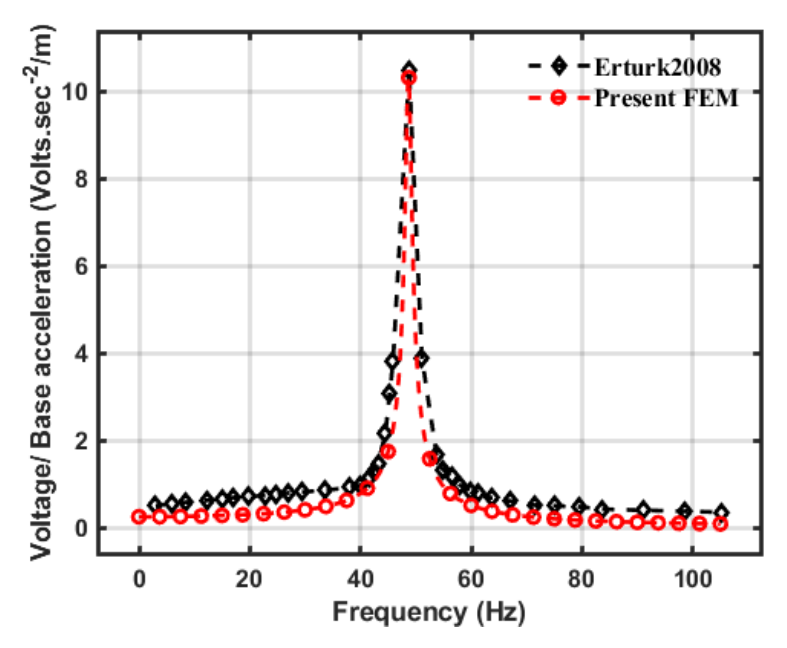


Figure 20. Validation of energy harvester model by comparing the voltage per unit base acceleration.

References

- 1. Mateu, L. and F. Moll. *Review of energy harvesting techniques and applications for microelectronics*. International Society for Optics and Photonics.
- 2. Riaz, A., et al., Review on Comparison of Different Energy Storage Technologies Used in Micro-Energy Harvesting, WSNs, Low-Cost Microelectronic Devices: Challenges and Recommendations. Sensors, 2021. **21**(15).
- 3. Xiong, C., et al., *Li–Na metal compounds inserted into porous natural wood as a bifunctional hybrid applied in supercapacitors and electrocatalysis.* International Journal of Hydrogen Energy, 2022. **47**(4): p. 2389-2398.
- 4. Chen, X., et al., *Nickel and cobalt sulfide-based nanostructured materials for electrochemical energy storage devices*. Chemical Engineering Journal, 2021. **409**: p. 127237-127237.
- 5. Hu, L., et al., *Highly conductive paper for energy-storage devices*. Proceedings of the National Academy of Sciences, 2009. **106**(51): p. 21490 LP-21494.
- 6. Iqbal, M.Z., M.M. Faisal, and S.R. Ali, *Integration of supercapacitors and batteries towards high-performance hybrid energy storage devices*. International Journal of Energy Research, 2021. **45**(2): p. 1449-1479.
- 7. Liang, T., et al., *The Applications of Water-in-Salt Electrolytes in Electrochemical Energy Storage Devices*. Advanced Functional Materials, 2021. **31**(3): p. 2006749-2006749.
- 8. Liu, Y., et al., Rechargeable aqueous Zn-based energy storage devices. Joule, 2021. 5(11): p. 2845-2903.
- 9. Gould, C. and R. Edwards. *Review on micro-energy harvesting technologies*. in 2016 51st International Universities Power Engineering Conference (UPEC). 2016.
- 10. Pandey, R., et al., Mutual Insight on Ferroelectrics and Hybrid Halide Perovskites: A Platform for Future Multifunctional Energy Conversion. Advanced Materials, 2019. **31**(43): p. 1807376-1807376.

- 11. Bowen, C.R., et al., *Piezoelectric and ferroelectric materials and structures for energy harvesting applications*. Energy and Environmental Science, 2014. **7**(1): p. 25-44.
- 12. Sodano, H.A., D.J. Inman, and G. Park, *A review of power harvesting from vibration using piezoelectric materials*. Shock and Vibration Digest, 2004. **36**(3): p. 197-206.
- 13. Priya, S., et al., A Review on Piezoelectric Energy Harvesting: Materials, Methods, and Circuits. Energy Harvesting and Systems, 2017. **4**(1): p. 3-39.
- 14. Setter, N., Piezoelectric materials in devices: extended reviews on current and emerging piezoelectric materials, technology, and applications. 2002: Ceramics Laboratory, EPFL Swiss Federal Institute of Technology.
- 15. Newnham, R.E., D.P. Skinner, and L.E. Cross, *Connectivity and piezoelectric-pyroelectric composites*. Materials Research Bulletin, 1978. **13**(5): p. 525-536.
- 16. Hagood, N.W. and A.A. Bent. *Development of piezoelectric fiber composites for structural actuation*.
- 17. Anton, S.R. and H.A. Sodano, *A review of power harvesting using piezoelectric materials* (2003-2006). Smart Materials and Structures, 2007. **16**(3): p. 197-206.
- 18. Hagood, N. and A. Bent. Development of piezoelectric fiber composites for structural actuation.
- 19. Setter, N., Piezoelectric materials in devices: extended reviews on current and emerging piezoelectric materials technology, and applications. 2003: Ceramics Laboratory, EPFL Swiss Federal Institute of Technology. 518-518.
- 20. Kim, H.S., J.H. Kim, and J. Kim, *A review of piezoelectric energy harvesting based on vibration*. International Journal of Precision Engineering and Manufacturing, 2011. **12**(6): p. 1129-1141.
- 21. Haddab, Y., N. Chaillet, and A. Bourjault. *A microgripper using smart piezoelectric actuators*. IEEE.
- 22. Yoon, K.J., et al., *Analytical design model for a piezo-composite unimorph actuator and its verification using lightweight piezo-composite curved actuators*. Smart Materials and Structures, 2004. **13**(3): p. 459-467.
- 23. Vaish, R., *Piezoelectric and pyroelectric materials selection*. International Journal of Applied Ceramic Technology, 2013. **10**(4): p. 682-689.
- 24. Vats, G. and R. Vaish, *Piezoelectric material selection for transducers under fuzzy environment*. Journal of Advanced Ceramics, 2013. **2**(2): p. 141-148.
- 25. Vats, G. and R. Vaish, *Selection of lead-free piezoelectric ceramics*. International Journal of Applied Ceramic Technology, 2014. **11**(5): p. 883-893.
- 26. Panda, P.K. and B. Sahoo, *PZT to lead free piezo ceramics: A review*. Ferroelectrics, 2015. **474**(1): p. 128-143.
- 27. Zhang, Y., H. Sun, and W. Chen, *A brief review of Ba(Ti0.8Zr0.2)O3-(Ba0.7Ca0.3)TiO3 based lead-free piezoelectric ceramics: Past, present and future perspectives.* Journal of Physics and Chemistry of Solids, 2018. **114**: p. 207-219.
- 28. Zhang, Y., et al., Dielectric and piezoelectric properties of porous lead-free 0.5Ba(Ca0.8Zr0.2)O3-0.5(Ba0.7Ca 0.3)TiO3 ceramics. Materials Research Bulletin, 2019. 112: p. 426-431.
- 29. Kiran, R., et al., Finite Element Study on Performance of Piezoelectric Bimorph Cantilevers Using
 Porous/Ceramic 0–3 Polymer Composites. Journal of Electronic Materials, 2018. **47**(1): p. 233-241.

- 30. Karmakar, S., et al., Effect of Porosity on Energy Harvesting Performance of 0.5Ba(Ca0.8Zr0.2)O3 0.5(Ba0.7Ca0.3)TiO3 Ceramics: A Numerical Study. Energy Technology, 2020. 8(5): p. 1901302-1901302.
- 31. Wang, P., Y. Li, and Y. Lu, Enhanced piezoelectric properties of (Ba0.85Ca0.15)(Ti0.9Zr0.1)O3 lead-free ceramics by optimizing calcination and sintering temperature. Journal of the European Ceramic Society, 2011. **31**(11): p. 2005-2012.
- 32. Karmakar, S., et al., Effect of sintering temperature on sensing, actuation and energy harvesting performance of (Ba0. 85Ca0. 15)(Ti0. 9Zr0. 1) O3 ceramics: A numerical and simulation based study. Engineering Research Express, 2021. 3(2): p. 25018-25018.
- 33. Huang, C. and L. Chen, *Negative Poisson's ratio in modern functional materials*. Advanced Materials, 2016. **28**(37): p. 8079-8096.
- 34. Ng, C.K., et al., On the anisotropic and negative thermal expansion from dual-material re-entrant-type cellular metamaterials. Journal of materials science, 2017. **52**(2): p. 899-912.
- 35. Han, Y., et al., *Unprecedented mechanical response of the lattice thermal conductivity of auxetic carbon crystals*. Carbon, 2017. **122**: p. 374-380.
- 36. Ren, X., et al., *Design and characterisation of a tuneable 3D buckling-induced auxetic metamaterial*. Materials & Design, 2018. **139**: p. 336-342.
- 37. Ren, X., et al., Experiments and parametric studies on 3D metallic auxetic metamaterials with tuneable mechanical properties. Smart Materials and Structures, 2015. **24**(9): p. 95016-95016.
- 38. Lakes, R., Foam structures with a negative Poisson's ratio. Science, 1987. 235: p. 1038-1041.
- 39. Evans, K.E., et al., *Molecular network design*. Nature, 1991. **353**(6340): p. 124-124.
- 40. Choi, J.B. and R.S. Lakes, *Non-linear properties of metallic cellular materials with a negative Poisson's ratio.* Journal of Materials Science, 1992. **27**(19): p. 5375-5381.
- 41. Argatov, I.I., R. Guinovart-Díaz, and F.J. Sabina, *On local indentation and impact compliance of isotropic auxetic materials from the continuum mechanics viewpoint.* International Journal of Engineering Science, 2012. **54**: p. 42-57.
- 42. Coenen, V.L. and K.L. Alderson, *Mechanisms of failure in the static indentation resistance of auxetic carbon fibre laminates.* physica status solidi (b), 2011. **248**(1): p. 66-72.
- 43. Choi, J.B. and R.S. Lakes, *Fracture toughness of re-entrant foam materials with a negative Poisson's ratio: experiment and analysis.* International Journal of fracture, 1996. **80**(1): p. 73-83.
- 44. Hou, W., et al., *Design of energy-dissipating structure with functionally graded auxetic cellular material.* International Journal of Crashworthiness, 2018. **23**(4): p. 366-376.
- 45. Hou, S., et al., *How does negative Poisson's ratio of foam filler affect crashworthiness?* Materials & Design, 2015. **82**: p. 247-259.
- 46. Alderson, A. and K.L. Alderson, *Auxetic materials*. Proceedings of the Institution of Mechanical Engineers, Part G: Journal of Aerospace Engineering, 2007. **221**(4): p. 565-575.
- 47. Evans, K.E., *Auxetic polymers: a new range of materials.* Endeavour, 1991. **15**(4): p. 170-174.
- 48. Topolov, V.Y. and C.R. Bowen, *Characteristics of 1–3-type ferroelectric ceramic/auxetic polymer composites*. Modelling and Simulation in Materials Science and Engineering, 2007. **16**(1): p. 015007.

- 49. Krishnaswamy, J.A., et al., *Design of polymeric auxetic matrices for improved mechanical coupling in lead-free piezocomposites*. Smart Materials and Structures, 2020. **29**(5): p. 54002-54002.
- 50. Alderson, K.L., et al., *Novel fabrication route for auxetic polyethylene. Part 1. Processing and microstructure.* Polymer Engineering and Science, 2005. **45**(4): p. 568-578.
- 51. Chan, H.L.W. and J. Unsworth, *Simple Model for Piezoelectric Ceramic/Polymer 1–3 Composites Used in Ultrasonic Transducer Applications*. IEEE Transactions on Ultrasonics, Ferroelectrics, and Frequency Control, 1989. **36**(4): p. 434-441.
- 52. Smith, W.A. and B.A. Auld, *Modeling 1–3 Composite Piezoelectrics: Thickness-Mode Oscillations*. IEEE Transactions on Ultrasonics, Ferroelectrics, and Frequency Control, 1991. **38**(1): p. 40-47.
- 53. Bisegna, P. and R. Luciano, *Variational bounds for the overall properties of piezoelectric composites*. Journal of the Mechanics and Physics of Solids, 1996. **44**(4): p. 583-602.
- 54. Bisegna, P. and R. Luciano, *On methods for bounding the overall properties of periodic piezoelectric fibrous composites*. Journal of the Mechanics and Physics of Solids, 1997. **45**(8): p. 1329-1356.
- 55. Cleveringa, H.H.M., E. Van Der Giessen, and A. Needleman, *Comparison of discrete dislocation and continuum plasticity predictions for a composite material*. Acta Materialia, 1997. **45**(8): p. 3163-3179.
- 56. Gaudenzi, P., *On the electromechanical response of active composite materials with piezoelectric inclusions.* Computers and Structures, 1997. **65**(2): p. 157-168.
- 57. Gunawardena, S.R., S. Jansson, and F.A. Leckie, *Modeling of anisotropic behavior of weakly bonded fiber reinforced MMC's*. Acta Metallurgica et Materialia, 1993. **41**(11): p. 3147-3156.
- 58. Barulich, N.D., L.A. Godoy, and P.M. Dardati, *A computational micromechanics approach to evaluate elastic properties of composites with fiber-matrix interface damage*. Composite Structures, 2016. **154**: p. 309-318.
- 59. Berger, H., et al., *Unit cell models of piezoelectric fiber composites for numerical and analytical calculation of effective properties*. Smart Materials and Structures, 2006. **15**(2): p. 451-458.
- 60. Berger, H., et al., *An analytical and numerical approach for calculating effective material coefficients of piezoelectric fiber composites.* International Journal of Solids and Structures, 2005. **42**(21-22): p. 5692-5714.
- 61. Kamiński, M., *Multiscale homogenization of n-component composites with semi-elliptical random interface defects.* International Journal of Solids and Structures, 2005. **42**(11): p. 3571-3590.
- 62. Sokołowski, D. and M. Kamiński, *Computational homogenization of carbon/polymer composites with stochastic interface defects*. Composite Structures, 2018. **183**: p. 434-449.
- 63. Sokołowski, D. and M. Kamiński, *Homogenization of carbon/polymer composites with anisotropic distribution of particles and stochastic interface defects*. Acta Mechanica, 2018. **229**(9): p. 3727-3765.
- 64. Database, C.M.M., Materials Database v4. 3.
- 65. Tuan, D.A., et al., Ferroelectric and piezoelectric properties of lead-free BCT-xBZT solid solutions. Materials Transactions, 2015. **56**(9): p. 1370-1373.
- 66. De Medeiros, R., et al., *Numerical and analytical analyses for active fiber composite piezoelectric composite materials*. Journal of Intelligent Material Systems and Structures, 2015. **26**(1): p. 101-118.

- 67. Melnykowycz, M., et al., *Performance of integrated active fiber composites in fiber reinforced epoxy laminates*. Smart Materials and Structures, 2006. **15**(1): p. 204-212.
- 68. Poizat, C. and M. Sester, *Finite element modelling of passive damping with resistively shunted piezocomposites*. Computational Materials Science, 2000. **19**(1-4): p. 183-188.
- 69. Teply, J.L. and G.J. Dvorak, *Bounds on overall instantaneous properties of elastic-plastic composites*. Journal of the Mechanics and Physics of Solids, 1988. **36**(1): p. 29-58.
- 70. Berger, H., et al. *An analytical and numerical approach for calculating effective material coefficients of* piezoelectric fiber composites. Pergamon. 742
- 71. Suquet, P.M., *Elements of Homogenization Theory for Inelastic Solid Mechanics*. Homogenization Techniques for Composite Media, 1987. **272**(September): p. 194-278.
- 72. Xia, Z., Y. Zhang, and F. Ellyin, *A unified periodical boundary conditions for representative volume elements of composites and applications*. International Journal of Solids and Structures, 2003. **40**(8): p. 1907-1921.
- 73. Benjeddou, A., *Advances in piezoelectric finite element modeling of adaptive structural elements: a survey.* Computers and Structures, 2000. **76**(1): p. 347-363.
- 74. Kim, J., V.V. Varadan, and V.K. Varadan, *Finite element modelling of structures including piezoelectric active devices*. International Journal for Numerical Methods in Engineering, 1997. **40**(5): p. 817-832.
- 75. Kumar, A., et al., Finite element analysis of vibration energy harvesting using lead-free piezoelectric materials: A comparative study. Journal of Asian Ceramic Societies, 2014. **2**(2): p. 138-143.
- 76. Narayanan, S. and V. Balamurugan. *Finite element modelling of piezolaminated smart structures for active vibration control with distributed sensors and actuators*. Academic Press.
- 77. Xu, S.X. and T.S. Koko, Finite element analysis and design of actively controlled piezoelectric smart structures. Finite Elements in Analysis and Design, 2004. **40**(3): p. 241-262.
- 78. Pinto Correia, I.F., et al. *Active control of axisymmetric shells with piezoelectric layers: A mixed laminated theory with a high order displacement field.* Pergamon.
- 79. Tan, X.G. and L. Vu-Quoc, *Optimal solid shell element for large deformable composite structures with piezoelectric layers and active vibration control.* International Journal for Numerical Methods in Engineering, 2005. **64**(15): p. 1981-2013.
- 80. Wang, C.Y. and R. Vaicaitis, *Active control of vibrations and noise of double wall cylindrical shells*. Journal of Sound and Vibration, 1998. **216**(5): p. 865-888.
- 81. Kumar, R., B.K. Mishra, and S.C. Jain, *Static and dynamic analysis of smart cylindrical shell*. Finite Elements in Analysis and Design, 2008. **45**(1): p. 13-24.
- 82. Karmakar, S., et al., Improved piezoelectric performance of 0.965 (K0.48Na0.52)(Nb0.96Sb0.04)O3 0.035Bi0.5Na0.5Zr0.15Hf0.75O3 piezocomposites using inherently auxetic polyethylene matrix. Applied Physics A, 2021. **127**(12): p. 965.
- 83. Jones, R.M., Mechanics of composite materials. 2nd ed. 2018: CRC press. 538.
- 84. Kim, S.B., et al., *Comparison of MEMS PZT cantilevers based on d31 and d 33 modes for vibration energy harvesting.* Journal of Microelectromechanical Systems, 2013. **22**(1): p. 26-33.

- 85. Xu, R. and S.-G. Kim, Figures of Merits of Piezoelectric Materials in Energy Harvesters. PowerMEMS, 2012: p. 464-467.
- 86. Bertoldi, K., et al., *Negative poisson's ratio behavior induced by an elastic instability*. Advanced Materials, 2010. **22**(3): p. 361-366.
- 87. Lakes, R., Advances in negative poisson's ratio materials. Advanced Materials, 1993. **5**(4): p. 293-296.
- 88. Bowen, C.R., et al., Fabrication and finite element modelling of interdigitated electrodes. Ferroelectrics, 1999. **228**(1): p. 257-269.
- 89. Bowen, C.R., et al., *Optimisation of interdigitated electrodes for piezoelectric actuators and active fibre composites*. Journal of Electroceramics, 2006. **16**(4): p. 263-269.
- 90. Kim, H., et al., Increased piezoelectric response in functional nanocomposites through multiwall carbon nanotube interface and fused-deposition modeling three-dimensional printing. MRS Communications, 2017. 7(4): p. 960-966.
- 91. Miki, M. and Y. Murotsu, *The Peculiar Behavior of the Poisson's Ratio of Laminated Fibrous Composites*. JSME international journal. Ser. 1, Solid mechanics, strength of materials, 1989. **32**(1): p. 67-72.
- 92. Milton, G.W., *Composite materials with poisson's ratios close to 1*. Journal of the Mechanics and Physics of Solids, 1992. **40**(5): p. 1105-1137.
- 93. Nkansah, M.A., K.E. Evans, and I.J. Hutchinson, *Modelling the effects of negative Poisson's ratios in continuous-fibre composites*. Journal of Materials Science, 1993. **28**(10): p. 2687-2692.
- 94. Alderson, K.L., et al., *How to make auxetic fibre reinforced composites*. physica status solidi (b), 2005. **242**(3): p. 509-518.
- 95. Webber, R.S., K.L. Alderson, and K.E. Evans, *A novel fabrication route for auxetic polyethylene, part 2: Mechanical properties.* Polymer Engineering & Science, 2008. **48**(7): p. 1351-1358.
- 96. Subramani, P., et al., Development of novel auxetic structures based on braided composites. Materials & Design, 2014. **61**: p. 286-295.
- 97. Erturk, A. and D.J. Inman, *A distributed parameter electromechanical model for cantilevered piezoelectric energy harvesters.* Journal of Vibration and Acoustics, Transactions of the ASME, 2008. **130**(4).